Original article

Silybin A from *Silybum marianum* reprograms lipid metabolism to induce a cell fate-dependent class switch from triglycerides to phospholipids

Solveigh C. Koeberle[a,b†,*], Maria Thürmer[c,†], Fengting Su[a,b], Markus Werner[c], Julia Grander[b], Laura Hofer[b], André Gollowitzer[b], Loc Le Xuan[b], Felix J. Benscheid[b], Ehsan Bonyadi Rad[b], Armando Zarrelli[d], Giovanni Di Fabio[d], Oliver Werz[c], Valeria Romanucci[d], Amelie Lupp[e], Andreas Koeberle[a,b,c*]

* Corresponding authors: Andreas Koeberle, University of Graz, Graz, 8010, Austria.

Solveigh C. Koeberle, University of Graz, Graz, 8010, Austria.

[a] *Institute of Pharmaceutical Sciences/Pharmacognosy and Excellence Field BioHealth, University of Graz, 8010 Graz, Austria*
[b] *Michael Popp Institute and Center for Molecular Biosciences Innsbruck (CMBI), University of Innsbruck, 6020 Innsbruck, Austria*
[c] *Department of Pharmaceutical/Medicinal Chemistry, Institute of Pharmacy, Friedrich Schiller University Jena, 07743 Jena, Germany*
[d] *Department of Chemical Sciences, University of Napoli Federico II, Naples, Italy*
[e] *Institute of Pharmacology and Toxicology, Jena University Hospital, Jena, Germany*

[†] These authors made equal contributions to this work.

*Corresponding authors. +43 316 380 - 8630.
E-mail addresses: andreas.koeberle@uni-graz.at (Andreas Koeberle).
solveigh.koeberle@uni-graz.at (Solveigh Koeberle).

Running title: The flavonolignan silybin favorably redistributes lipids

Abstract

Rationale: *Silybum marianum* is used to protect against degenerative liver damage. The molecular mechanisms of its bioactive component, silybin, remained enigmatic, although membrane-stabilizing properties, modulation of membrane protein function, and metabolic regulation have been discussed for decades.

Methods: Experiments were performed with hepatocyte cell lines and primary monocytes *in vitro* under both basal and stressed conditions, and in mice *in vivo*. Quantitative lipidomics was used to detect changes in phospholipids and triglycerides. Key findings were confirmed by Western blotting, quantitative PCR, microscopy, enzyme activity assays, metabolic flux studies, and functional relationships were investigated using selective inhibitors.

Results: We show that specifically the stereoisomer silybin A decreases triglyceride levels and lipid droplet content, while enriching major phospholipid classes and maintaining a homeostatic phospholipid composition in human hepatocytes *in vitro* and in mouse liver *in vivo* under normal and pre-disease conditions. Conversely, in cell-based disease models of lipid overload and lipotoxic stress, silybin treatment primarily depletes triglycerides. Mechanistically, silymarin/silybin suppresses phospholipid-degrading enzymes, induces phospholipid biosynthesis to varying degrees depending on the conditions, and down-regulates triglyceride remodeling/biosynthesis, while inducing complex changes in sterol and fatty acid metabolism. Structure-activity relationship studies highlight the importance of the 1,4-benzodioxane ring configuration of silybin A in triglyceride reduction and the saturated 2,3-bond of the flavanonol moiety in phospholipid accumulation. Enrichment of hepatic phospholipids and intracellular membrane expansion are associated with a heightened biotransformation capacity.

Conclusion: Our study deciphers the structural features of silybin contributing to hepatic lipid remodeling and suggests that silymarin/silybin protects the liver in individuals with mild

metabolic dysregulation, involving a lipid class switch from triglycerides to phospholipids, whereas it may be less effective in disease states associated with severe metabolic dysregulation.

KEY WORDS silybin, liver, lipid metabolism, triglycerides, phospholipids

Introduction

Hepatic pathologies such as metabolic dysfunction-associated steatotic liver disease (MAFLD; former: non-alcoholic fatty liver disease, NAFLD [1]), metabolic dysfunction-associated steatohepatitis (MASH; former: non-alcoholic steatohepatitis, NASH), fibrosis, and cirrhosis are closely related to the metabolic syndrome and insulin resistance [2-6]. They are driven by high-calorie diets that induce abnormal glucose and lipid metabolism and subsequently cause glucotoxicity, lipotoxicity, oxidative stress, and chronic inflammation [2,7-9]. As a consequence, fatty acids are taken up by hepatocytes, and also synthesized *de novo* [10], incorporated into triglycerides (TGs), and stored in lipid droplets [11-13]. While the transfer of fatty acids into lipid droplets contributes to the detoxification of excess free fatty acids [13], a chronic increase in the number and size of lipid droplets induces hepatocyte enlargement and dysfunction [7,14]. This continuous lipid accumulation leads to hepatic steatosis and, as the disease progresses, to cirrhosis and hepatocellular carcinoma [2,15]. As an adaptive strategy to protect hepatocytes from lipid overload, autophagy of lipid droplets (lipophagy) is initiated [16] and the mobilized fatty acids are subjected to oxidative degradation [17]. Compensatory upregulation of fatty acid oxidation at the onset of MAFLD provides partial relief but is insufficient to reduce hepatic lipids to basal levels. In addition, the increased oxidative breakdown of lipids induces oxidative stress, which can negatively contribute to cell and tissue damage [7,18]. MAFLD is also significantly influenced by genetic factors [19]. Candidate gene variants act in multiple pathways of lipid metabolism [20], including *de novo* lipogenesis and lipid droplet assembly (LPIN2, ATGL/PNPLA2)[21,22], phospholipid biosynthesis and remodeling (LPIAT1/MBOAT7, iPLA2/PLA2G6, PNPLA8, PRDX6, PLD1)[23-29], neutral and phospholipid hydrolysis and catabolism (PNPLA3)[30], sterol metabolism (HSD17B13)[31] fatty acid compartmentalization (GCKR, TM6SF2), and lipoprotein assembly and secretion (PLA2G7,

TM6SF2)[26]. Consequently, both MAFLD and MASH are characterized by extensive changes in hepatic lipid composition, including a decrease in total phosphatidylcholine (PC) and an increase in TG [32-35].

Milk thistle (*Silybum marianum* L.) is a medicinal plant that is traditionally used for the treatment of liver and biliary tract diseases [36-39] and a variety of other pathologies, including diabetes [40] and cancer [41,42]. Organic fruit extracts (silymarin) of *S. marianum* consist of the flavonolignans silybin A and B (~30%), isosilybin (~5%), silychristin A (~7%), and silydianin (~10%), the flavonoid (+)-taxifolin (~5%) (Figure 1A), and less defined polyphenols (30%) [41,43]. Minor constituents include silychristin B, isosilychristin, 2,3-dehydrosilybin, quercetin, and kaempferol [41,43,44]. The major biologically active flavonolignan, silybin, also termed as silibinin, exists as a mixture of the two diastereomers silybin A and B [43]. Human and animal studies with silymarin or its main component silybin on liver pathologies such as oxidative or lipotoxic stress-induced alcoholic and non-alcoholic fatty liver disease and steatohepatitis show (pre)clinical efficacy [45-49], whereas studies on xenobiotic-induced liver toxicity produced mixed results [36,38,50], with only rare cases of side effects [51]. Note that the oral bioavailability of silybin can be substantially boosted by specific formulations, yielding systemic silybin plasma concentrations (C_{max}) up to 85 µM in humans [36]. The hepatoprotective activities of silymarin/silybin have been ascribed to antioxidant response inducing, anti-inflammatory [52], antifibrotic, hepatocyte regeneration-stimulating, and membrane-stabilizing properties [47,53]. Several studies have found that administration of silymarin/silybin reduces levels of low-density lipoprotein (LDL), VLDL, cholesterol, and/or TGs, while other studies have not observed substantial changes in the serum lipid profile [54-59], which is not readily understood but may be related to the dose. Recently, silymarin (but not silybin) has been proposed to decrease lipid accumulation during a high-fat diet by altering the vitamin B12-producing capacity of the gut microbiota [60]. On

the other hand, silymarin/silybin has been suggested to increase PC biosynthesis by upregulating choline phosphate cytidylyltransferase [61]. Silymarin/silybin compensated for the decrease of phosphatidylcholine (PC) and phosphatidylethanolamine (PE) in rat liver upon intoxication [62,63] and, when given as a silybin- and PC-based food integrator to MASH patients, restored plasma PC and sphingomyelin (SM) levels [54]. Whether silymarin/silybin actively promotes phospholipid enrichment or indirectly increases phospholipid levels by alleviating disease conditions is insufficiently understood, as are the consequences for other membrane phospholipid classes and the knowledge of phospholipidomic profiles. The latter is of great importance because imbalances in the membrane phospholipid composition can cause severe alterations in membrane architecture and function [64].

Here, we demonstrate that silymarin/silybin increases the levels of phospholipids by suppressing their degradation. This effect is partially combined with the induction of phospholipid biosynthetic enzymes, depending on the condition. Simultaneously, it reduces TG levels by downregulating multiple biosynthetic enzymes or by altering TG remodeling processes in hepatocytes, depending on the specific context. To some extent, this effect is also observed in extrahepatic cell types. We ascribe this activity to specific structural features of silybin A and find that they prevail in healthy or pre-disease states not yet afflicted with massive lipid overload, whereas TG-lowering mechanisms predominate under the latter severe liver disease conditions. The channeling of fatty acids from triglycerides to phospholipids has the advantage of i) reducing hepatic TG levels and lipid droplet size ii) avoiding high lipotoxic levels of free fatty acids, and iii) expanding intracellular membranes, which may explain the enhanced hepatic biotransformation capacity upon treatment with silybin. Major adverse changes in membrane function are not expected from the balanced upregulation of phospholipid species. Conclusively, our data suggest that the mechanism of

137 silymarin/silybin described here is more effective in protecting against metabolic liver disease
138 rather than reversing advanced disease states.

139 **Materials and Methods**

140 *Materials*

141 Silybin, staurosporine, and atglistatin were obtained from Merck (Darmstadt, Germany),
142 silybin-C-2',3-bis(hydrogen succinate) disodium salt (Legalon® SIL) was from Madaus
143 GmbH (Köln, Germany), the PPARγ antagonist GW9662, and the DGAT1 inhibitor A-
144 922500 were purchased from Cayman Chemicals (Ann Arbor, MI), the DGAT2 inhibitor PF-
145 06424439 was bought from Bio-Techne (Abingdon, United Kingdom), thapsigargin was from
146 Enzo Life Sciences (Farmingdale, NY), and silymarin (Silimarit®) was a kind gift from
147 Bionorica SE (Neumarkt, Germany). Silybin, its derivatives and other compounds were
148 dissolved in DMSO, stored in the dark at -20°C under argon, and freezing/thawing cycles
149 were kept to a minimum. Silymarin was freshly dissolved in ethanol at the day of experiment.
150 Phospholipid standards were purchased from Otto Nordwald GmbH (Hamburg, Germany) or
151 Merck Millipore (Darmstadt, Germany), were dissolved in chloroform, aliquoted and stored
152 under argon protected from light at -80°C. BODIPY 493/503 and ProLong™ Diamond
153 Antifade Mountant with DAPI were purchased from Thermo Fisher Scientific (Waltham,
154 MA). Rabbit anti-β-actin (13E5; #4970), mouse anti-β-actin (8H10D10; #3700), rabbit anti-
155 acetyl-CoA carboxylase (C83B10; #3676), rabbit anti-ATF-6 (D4Z8V, #65880), rabbit anti-
156 ATGL (#2138), rabbit anti-BiP (C50B12, #3177), rabbit anti-phospho-acetyl-CoA
157 carboxylase (Ser79; D7D11; #11818), rabbit anti-GAPDH (D16H11; #5174), mouse anti-
158 GAPDH (D4C6R; #97166), rabbit anti-FAS (#3189), and rabbit anti-XBP-1s (D2C1F,
159 #12782S) were obtained from Cell Signaling (Danvers, MA). Mouse anti-calnexin (C8.B6;
160 #MAB3126) was from Merck Millipore (Darmstadt, Germany) and mouse anti-GM130

(#610822) from BD Bioscience (San Jose, CA, USA). Goat anti-rat CYP1A1 (#219207), goat anti-rat CYP3A2, (#210167), and goat anti-rat CYP2B1, (#219207) were obtained from Daiichi Pure Chemicals Co. LTD (Tokyo, Japan). Rabbit anti-DGAT1 (NB110-41487SS) and rabbit anti-DGAT2 (NBP1-71701SS) were from Novus Biologicals (Abingdon, UK). Mouse anti-GRP78/BiP (A-10, #sc-376768) was purchased from Santa Cruz Biotechnology (Dallas, TX). Alexa Fluor 555 goat anti-mouse IgG (H+L) and Alexa Fluor 488 goat anti-rabbit IgG (H+L) were purchased from Life Technologies (MA, USA). Secondary antibodies for Western blot studies were from LI-COR Biosciences (Bad-Homburg, Germany) and Thermo Fisher Scientific. Peroxidase-conjugated avidin and the secondary biotinylated antibodies rabbit anti-mouse IgG and rabbit fblanti-goat used in immunohistochemical studies were from VECTASTAIN® Elite ABC-Kit (Vector Laboratories, Burlingame, CA)

Synthesis of silybin derivatives

Silybin A and B were separated from the diastereomeric mixture silybin (Merck) by preparative HPLC as described[65]. Starting from the purified silybin A and B, the two enantiomers of 2,3-dehydrosilybin (A and B) were synthesized in good yields and optically pure by base-catalyzed oxidation under microwave heating [66]. The hemiacetal **11**, was obtained in good yield by the microwave conversion of silybin in pyridine at 110°C [66]. All products were fully characterized by NMR (^{1}H, ^{13}C), CD, $[\alpha]_D$, and ESI MS analyses. The purities of the products were higher than 98%.

Cell culture, primary monocytes and cell treatment

Cultured cell lines: Human HepG2 liver carcinoma cells (1×10^5 cells/cm^2, Leibniz Institute DSMZ-German Collection of Microorganisms and Cell Cultures, Braunschweig, Germany) were grown in RPMI 1640 medium containing 10% heat-inactivated fetal calf serum (FCS, GE Healthcare, Freiburg, Germany or Merck) at 37°C and 5% CO_2. Human HepaRG

hepatoma cells (1.5-2×10^5 cells/cm^2, Biopredic International, Rennes, France) were cultured in William's E medium (Merck) supplemented with 10% heat-inactivated FCS, 2 mM *L*-glutamine (Merck), 5 µg/ml human insulin (Merck), and 50 µM hydrocortisone (Cayman) at 37°C and 5% CO_2. Human Caco-2 colorectal adenocarcinoma cells (1.7×10^5 cells/cm^2) were cultured in DMEM medium (Merck) containing 10% FCS at 37°C and 5% CO_2. Cells were detached by trypsin/EDTA and reseeded every 3-4 days before reaching confluence. HepG2 cells were used up to passage 28 and HepaRG cells up to passage 44.

Primary cells: Collection of venous blood in heparinized tubes (16 I.E. heparin/mL blood) was performed by the Institute for Transfusion Medicine of the University Hospital Jena (Germany) with informed consent of registered male and female healthy adult volunteers (18 to 65 years). Blood donors were fasted for at least 12 h, had not taken antibiotics or anti-inflammatory drugs prior to blood donation (> 10 days), and were free of apparent infections, inflammatory disorders, or acute allergic reactions. The volunteers regularly donated blood (every 8 to 12 weeks) and were physically inspected by a clinician. Leukocyte concentrates were prepared, erythrocytes removed by dextran sedimentation, and peripheral blood mononuclear cells (PBMC) were isolated by density gradient centrifugation on lymphocyte separation medium (LSM 1077, GE Healthcare) as previously described[67]. The fraction of PBMC was cultivated in RPMI 1640 medium containing 10% FCS in 12-well plates (37°C, 5% CO_2) at a density of 2×10^7/ml for 1 to 1.5 h to separate adherent monocytes. The cell population used for further studies consisted of more than 85% monocytes according to forward and side scatter properties and CD14 surface expression (BD FACS Calibur flow cytometer, BD Biosciences, Heidelberg, Germany). Experiments were approved by the ethical commission of the Friedrich-Schiller-University Jena.

Cell treatment: HepG2 cells (1×10^5 cells/cm^2) and monocytes (6×10^5/cm^2) were seeded and directly exposed to vehicle (0.1% DMSO or 0.05% ethanol), silymarin (50 µg/ml for

monocytes and 10 µg/ml for HepG2 cells), silybin A/B (20 µM), or STS (1 µM). Adherent cells were harvested with trypsin/EDTA (Merck or Promega, Madison, WI). For lipid droplet staining with Oil Red O, HepG2 cells were instead seeded in 96-well plates at 20,000 cells per well and incubated for 24 h before treatment with vehicle (0.5% DMSO or 0.5% ethanol), silymarin (10 µg/ml), or silybin A/B (20 µM) for an additional 24 h. Treatment of HepaRG cells is described in section "*Cell-based models of MAFLD and lipotoxic stress*". For transcriptome analysis, Caco-2 cells (1.7×10^5 cells/cm^2) were seeded and directly exposed to vehicle (0.5% DMSO), silymarin (30 µg/ml), and silybin (30 µM) for 24 h. Adherent cells were harvested with trypsin/EDTA.

Complexation of fatty acids to BSA

BSA (1%, Carl Roth, Karlsruhe, Germany) was dissolved in Williams E medium, sterile filtered (Rotilabo®-syringe filter, PVDF, 0.22 µm, Carl Roth), mixed with PA (50 mM) or OA (50 mM), sonicated at 60°C for 30 min using a USC100TH sonicator (VWR, Vienna, Austria, 60 W, 45 kHz), and stored at -20°C. Solutions were mixed vigorously immediately before use.

Cell-based models of MAFLD and lipotoxic stress

HepaRG cells (10,000 / well, 96-well plate) or 2.5×10^6 cells/25 cm^2 were cultured at 37°C and 5% CO_2 for 24 h. The cell culture medium was replaced with fresh medium supplemented with i) vehicle (1% BSA in Williams E medium), ii) BSA-complexed PA/16:0 (0.1 mM, Merck) and OA/18:1 (Cayman) in a 1:2 ratio (in total 1 mM) to induce massive lipid accumulation (mimicking MAFLD), or iii) BSA-complexed PA (0.1 mM) to induce lipotoxic stress. For lipidomic analysis, cells were either co-treated directly with vehicle (DMSO, 0.5%) or silybin A (20 µM), and the incubation was prolonged for another 24 h. Alternatively, treatment was started 24 h after fatty acid challenge and incubation was prolonged for a

234 further 24 h. For lipid droplet analysis, cells were co-treated with vehicle (DMSO, 0.5%),
235 silybin A (20 µM), the ATGL inhibitor atglistatin (50 µM), the DGAT1 inhibitor A 922500 (5
236 µM), the DGAT2 inhibitor PF-06424439 (10 µM), a combination of DGAT1 (5 µM) and
237 DGAT2 inhibitors (10 µM), or the PPARγ antagonist GW9662 (5 µM) and the incubation
238 was prolonged for another 24 h or 48 h, respectively. Lipid droplet signals, the number of
239 viable cells and membrane integrity, cellular metabolic activity, and phospholipid and TG
240 levels were determined as described in sections 5.6, 5.7, 5.8, 5.10, and 5.11, respectively.

241 *Quantitation of lipid droplets in hepatocytes*

242 HepaRG cells were washed twice with 100 µl PBS pH 7.4 and fixed with paraformaldehyde
243 solution (4% in PBS pH 7.4, Merck) for 40 min at room temperature. After removal of the
244 fixative, the cells were washed twice with 100 µl of water, incubated with aqueous
245 isopropanol (60%, 100 µl, 5 min) to remove polar lipids and reduce background signals, and
246 stained with Oil Red O solution (50 µl) for 25 min at room temperature. The latter was
247 prepared by diluting 0.5% Oil Red O in isopropanol (Merck) 1.7-fold in water, sterile-filtered
248 (Rotilabo®-syringe filter, PVDF, 0.22 µm, Carl Roth), and allowed to stand for 10 min before
249 staining. Cells were washed three times with water, and microscopic images were taken using
250 a 40× objective (Motic, Barcelona, Spain) on a Motic AE31E microscope (Motic) equipped
251 with a Motic camera. Alternatively, lipid droplets in HepG2 cells were stained with BODIPY
252 493/503 and manually counted as described in section 5.15. For photometric quantitation of
253 the stained lipid droplets, Oil Red O was extracted with 60% isopropanol in water (100 µl) for
254 10 min at room temperature, and the absorbance of the extracted solution was measured at
255 510 nm using a multi-mode microplate reader (SpectraMax iD3, Molecular Devices).

Cell number, viability, morphology, and cell diameter

Cell number, cell viability, and cell diameters were determined after trypan blue staining using a Vi-CELL Series Cell Counter (Beckmann Coulter GmbH, Krefeld, DE). Morphological analysis of the cells was carried out on an Axiovert 200 M microscope with a Plan Neofluar × 100/1.30 Oil (DIC III) objective (Carl Zeiss, Jena, Germany). Images were obtained using an AxioCam MR3 camera (Carl Zeiss).

Cell viability based on cellular dehydrogenase activity

Cytotoxic effects of silymarin and silybin were determined as described [68]. Briefly, HepG2 cells (1×10^5/well of a 96-well plate) or HepaRG cells were cultured as described in sections 5.3. and 5.5. Cells were treated with silymarin, silybin, or vehicle (0.5% DMSO or 0.25% ethanol) at 37°C and 5% CO_2. The pan-kinase inhibitor staurosporine (1 µM) was used as reference compound. After 24 h, 3-(4,5-dimethylthiazol-2-yl)-2,5-diphenyltetrazolium bromide (MTT, 20 µl, 5 mg/ml, Merck) was added to each well, and cells were incubated for another 3 h (HepG2) or 2.5 h (HepaRG) at 37°C and 5% CO_2 before being lysed in SDS buffer (10% in 20 mM HCl, pH 4.5) overnight. The absorption of the solubilized formazan product was measured at 570 nm (Multiskan Spectrum, Thermo Fisher Scientific or SpectraMax iD3, Molecular Devices).

Extraction and analysis of phospholipids, neutral lipids, and fatty acids

To extract lipids from cell pellets (HepG2 cells, HepaRG cells, and monocytes) or supernatants of liver homogenates after centrifugation (9,000×g, 10 min, 4°C), PBS pH 7.4, methanol, chloroform, and saline (final ratio: 14:34:35:17) were added in succession [69,70]. Phospholipids, TGs and fatty acids in the lower organic phase were evaporated to dryness, dissolved in methanol, and analyzed by UPLC-MS/MS. Internal standards: 1-Pentadecanoyl-2-oleoyl(d7)-sn-glycero-3-phosphoethanolamine, 1-pentadecanoyl-2-oleoyl(d7)-sn-glycero-3-

phosphocholine, and/or 1,3-dipentadecanoyl-2-oleyol(d7)-glycerol were used for lipidomic analysis related to Figure 4, Figure 7 and Figure S13 and S14. Other samples contained 1,2-dimyristoyl-*sn*-glycero-3-phosphatidylcholine as internal standard, and 1,2-dimyristoyl-*sn*-glycero-3-phosphatidylethanolamine, 1,2-di-heptadecanoyl-*sn*-glycero-3-phosphatidyl-glycerol, and/or 1,2-diheptadecanoyl-*sn*-glycero-3-phosphoserine.

Phospholipids, CE, TGs, and free fatty acids were separated on an Acquity™ UPLC BEH C8 column (1.7 µm, 2.1×100 mm, Waters, Milford, MA, USA) using an Acquity™ Ultraperformance LC system (Waters) as described before [71-73]. Alternatively, phospholipids and TGs were separated by an ExionLC™ AD UHPLC (Sciex, Framingham, MA, USA) [74-76]. In brief, phospholipids were analyzed at a flow rate of 0.75 ml/min at 45°C using acetonitrile/water (95/5) and 2 mM ammonium acetate as mobile phase A and water/acetonitrile (90/10) and 2 mM ammonium acetate as mobile phase B. Mobile phase A was ramped from 75 to 85% within 5 min, followed by an increase to 100% within 2 min and isocratic elution for another 2 min. For the separation of TGs, mobile phase B was replaced by isopropanol, and the initial composition of mobile phase A was lowered from 90 to 70% within 6 min, which was succeeded by isocratic elution for 4 min.

Glycerophospholipids were detected by multiple reaction monitoring (MRM) in the negative ion mode based on their fatty acid anion fragments using a QTRAP 5500 [72] or QTRAP 6500^{+} [77]. Mass Spectrometer (Sciex), which were equipped with electrospray ionization (ESI) sources. For the analysis of PE and PC using the QTRAP 6500^{+} Mass Spectrometer (Figure 5, Figure S3, and Figure S14), the curtain gas was set to 40 psi, the collision gas was set to medium, the ion spray voltage was set to -4500 V, the heated capillary temperature was set to 650°C (PE) or to 350 °C (PC), the sheath gas pressure was set to 55 psi, the auxiliary gas pressure was set to 75 psi, the declustering potential was set to -50 V, the entrance

potential was set to -10 V, the collision energy was set to -38 eV, and the collision cell exit potential was set to -12 V [76].

CE and TGs were identified and quantified in the positive ion mode as NH_4^+ adduct ions that undergo neutral loss of either of the acyl groups [73]. When using the QTRAP 6500^+ Mass spectrometer (Figure 4, Figure 5, Figure S3, and Figure S13 and S14), the curtain gas was set to 30 psi (CE) or 40 psi (TG), the collision gas to low, the ion spray voltage to 5500 V, the heated capillary temperature to 350°C (CE) or 400°C (TG), the sheath gas pressure to 55 psi (CE) or 60 psi (TG), the auxiliary gas pressure to 70 psi, the declustering potential to 55 V (CE) 120 V (TG), the entrance potential to 10 V, the collision energy to 22 V (CE) or 35 eV (TG), and the collision cell exit potential to 22 V (CE) or 26 V (TG) [76]. Free fatty acids were analyzed by single ion monitoring in the negative ion mode [69] and SM by MRM in the positive ion mode based on the detection of the choline headgroup (m/z = 184)[69].

Absolute lipid quantities were normalized for Figure 4, Figure 5, S13 and S14 to lipid subclass-specific internal standards and cell number. For other experiments, lipid intensities were normalized to 1,2-dimyristoyl-sn-glycero-3-phosphatidylcholine and the number of cells to calculate the amounts in nmol / 10^6 cells (PC) or in relative units (other lipid subclasses). Relative intensities represent the percentage of individual lipid species relative to all lipid signals determined within the respective lipid class (= 100%). The most intensive or specific transition was used for quantitation. Analyst 1.6 or Analyst 1.7 (Sciex) were used to acquire and process mass spectra.

Extraction and analysis of acyl-CoAs

HepG2 cells were suspended in methanol/water (70/30) and placed at -20°C for 1 h. After vigorous mixing, the methanol/water ratio was adjusted to 50/50 and the samples were incubated for another hour at -20°C. Protein precipitates were removed by centrifugation

(20,000×g, 5 min, 4°C), and the supernatant was evaporated to dryness. The residue was extracted with methanol/water (50/50) and the extract subjected to UPLC-MS/MS analysis. [$^{13}C_3$]-Malonyl-CoA (1 nmol; Merck) was used as internal standard.

Acyl-CoAs were separated on an Acquity^{TM} UPLC BEH C18 column (1.7 µM, 2.1×50 mm) with an Acquity^{TM} Ultra Performance LC system [78] and analyzed by MRM in the positive ion mode following electrospray ionization (QTRAP 5500 mass spectrometer). Fragments formed by neutral loss of 2'-phospho-ADP ([M+H-507]$^+$) were detected for quantitation. The ion spray voltage was set to 3,000 V, the heated capillary temperature to 600°C, the curtain gas pressure to 30 psi, the sheath gas pressure to 45 psi, the auxiliary gas pressure to 55 psi, the declustering potential to 60 V, the entrance potential to 10 V, and the collision energy to 45 eV (malonyl-CoA) or 30 eV (other acyl-CoAs). Absolute lipid amounts are calculated with respect to the internal standard of the subclass and are normalized to cell number, protein content or tissue weight. Relative lipid proportions are expressed as a percentage of the total sum of all species detected within the corresponding subclass (equal to 100%). Mass spectra were acquired and analyzed using Analyst 1.6 or 1.7 (Sciex).

Metabolic flux studies

HepG2 cells (1×10^5 cells/cm^2) were seeded and directly treated with either vehicle control (0.05% ethanol or 0.1% DMSO), silymarin (10 µg/ml) or silybin A (20 µM) and cultured for 6 h at 37°C and 5% CO_2. Cells were treated with sodium acetate-$^{13}C_2$, d_3 (30 µM, Merck, #299111) for further 18 h before lipids were extracted and analyzed by UPLC-MS/MS as described above. PE species carrying 16:0-$^{13}C_2$, d_1, 18:0-$^{13}C_2$, d_1, 18:1-$^{13}C_2$, d_1, or 20:4-$^{13}C_2$, d_1 were quantified by MRM in the negative ion mode as transitions from [M+3+CH_3COO]$^-$ parental ions to the respective isotope-labeled and non-isotope-labeled fatty acid anions. TG species carrying 16:0-$^{13}C_2$, d_1, 18:0-$^{13}C_2$, d_1, 18:1-$^{13}C_2$, d_1, or 18:2-$^{13}C_2$, d_1 were detected by MRM in the positive ion mode as transitions from [M+3+NH_4]$^+$ parental ions to the respective

fragment anions following release of an isotope-labeled or non-isotope-labeled acyl group. In parallel, non-labeled TG and PE were analyzed to calculate the M+3 isotopic patterns from the monoisotopic signals using the Mass (m/z) calculation tool from Lipid Maps® (https://www.lipidmaps.org/tools/structuredrawing/masscalc.php). These isotopic signals were subtracted from the corresponding signals of the $^{13}C_2$, d_1 – labeled species.

Transcriptome analysis

Caco-2 cells (1.7×105 cells/cm^2) were treated with vehicle (0.5% DMSO), 30 µg/ml silymarin or 30 µM silybin for 24 h (n = 3 biological replicates). Total RNA was isolated using a RNeasy Mini Kit (Qiagen) and potential DNA contamination was digested with DNase I (Qiagen) during RNA purification according to the manufacturer's protocol. RNA concentration and quality were assessed using a SpectraMax iD3 microplate reader (Molecular Devices), a bioanalyzer (Agilent) and Qubit (Thermo Fisher Scientific) before being submitted to the MultiOmics Core Facility, Medical University of Innsbruck, for sequencing. The RNA integrity (RIN) of all samples was > 9.5 (out of 10) and no genomic DNA contamination was detected in any of the samples prior to RNA sequencing. Libraries were prepared using Lexogen's Quant Seq 3'mRNA Seq Library Kit FWD with UMI protocol (Lexogen GmbH, Vienna, Austria). Quality validated libraries were multiplexed and sequenced at 150 bp read length using Illumina NovaSeq technology and the generated paired-end raw sequence data reads were quality controlled using FastQC and MultiQC202 [79].

Sequencing adapters and reads shorter than 50 base pairs were removed using Trim Galore (Galaxy version 0.6.7) to improve mapping quality, and reads were mapped to the GRCh38 human reference genome (December 2013) using the RNAStar aligner (Galaxy version

2.7.10b)[80]. Final transcript count data were generated with HTSeq framework (Galaxy version 2.0.5)[81] for high-throughput sequencing data based on the Ensemble release Homo_sapiens.GRCh38.107 gene annotation with default settings. All analyses were performed on a public instance of Galaxy at usegalaxy.eu. Differential gene expression analysis was performed using DESeq2 package version 1.26[82] with an adjusted *P*-value < 0.05 (5% FDR).

In addition, we re-analyzed microarray-based transcriptome datasets: i) HepG2 cells treated with vehicle (0.0125% DMSO) or 12 µg/ml silymarin (Merck) for 24 h (n = 3 biological replicates)[83]; ii) Huh7.5.1 cells treated with vehicle (0.32% DMSO) or 40 µg/ml silymarin (Madaus Group, Cologne, Germany) for 4, 8, or 24 h (pooled triplicates in three [silymarin, 8 h; silymarin, 24 h], four [vehicle and silymarin, 4 h], or five [vehicle, 8 and 24 h] technical replicates)[84]; iii) primary human hepatocytes from chronically HCV-infected chimeric mice with humanized livers either untreated or receiving 469 mg/kg silybin-C-2',3-bis(hydrogen succinate) disodium salt (Legalon® SIL, in saline, all three mice on day 3 and two mice on day 14) or 265 mg/kg Legalon® SIL (in saline, one mouse on day 14) intravenously daily for 3 or 14 days (n = 3 mice/group)[85]. Data are accessible at NCBI GEO database[86], accessions GSE67504, GSE50994, and GSE79103. Differentially regulated genes were identified by pairwise comparison of treatment and control groups using the GEO2R interactive web tool (https://www.ncbi.nlm.nih.gov/geo/geo2r/)[86]. *P* values were calculated by multiple *t*-tests, either with or without correction for multiple comparisons according to Benjamini and Hochberg (false discovery rate 5%) and auto-detection for log-transformation.

Sample preparation, SDS-PAGE, and Western blotting

Pelleted and washed monocytes and HepG2 cells were lysed in ice-cold 20 mM Tris-HCl (pH 7.4), 150 mM NaCl, 2 mM EDTA, 1% Triton X-100, 5 mM sodium fluoride, 10 µg/ml leupeptin, 60 µg/ml soybean trypsin inhibitor, 1 mM sodium vanadate, 2.5 mM sodium

pyrophosphate, and 1 mM phenylmethanesulphonyl fluoride, and sonicated on ice (2 × 5 s, Q125 Sonicator, QSonica, Newtown, CT, 125 W, 35% amplitude). After centrifugation (cell lysates: 12,000×g, 5 min, 4°C; liver homogenates: 9,000×g, 10 min, 4°C), the protein concentration of the supernatants was determined using a DC protein assay kit (Bio-Rad Laboratories, CA). Samples (10-15 µg total protein) were combined with loading buffer (1×; 125 mM Tris-HCl pH 6.5, 25% sucrose, 5% SDS, 0.25% bromophenol blue, and 5% β-mercaptoethanol) and heated for 5 min at 95 °C. Proteins were separated by 8-10% SDS-PAGE and transferred to a Hybond ECL nitrocellulose membrane (GE Healthcare) or Amersham Protran 0.45 µm NC nitrocellulose membranes (Carl Roth, Karlsruhe, Germany). Membranes were blocked with 5% bovine serum albumin (BSA) or skim milk for 1 h at room temperature and incubated with primary antibodies overnight at 4°C. IRDye 800CW-labeled anti-rabbit IgG (1:10,000, 92632211, LI-COR Biosciences, Lincoln, NE), IRDye 800CW-labeled anti-mouse IgG (1:10,000, 926-32210, LI-COR Biosciences, Lincoln, NE), IRDye 680LT-labeled anti-rabbit IgG (1:80,000, 926-68021, LI-COR Biosciences, Lincoln, NE), IRDye 680LT-labeled anti-mouse IgG (1:80,000, 926-68020, LI-COR Biosciences, Lincoln, NE), DyLight® 680 goat anti-rabbit IgG (1:10,000, # 35569, Thermo Fisher Scientific), and/or DyLight® 800 goat anti-mouse IgG (1:10,000, # SA5-10176, Thermo Fisher Scientific) were used as secondary antibodies. Fluorescent, immunoreactive bands were visualized using an Odyssey infrared imager (LI-COR) or a Fusion FX7 Edge Imaging System (spectra light capsules: C680, C780; emission filters: F-750, F-850; VILBER Lourmat, Collegien, France) [74]. Acquired data from densitometric analysis were linearly adjusted and background-corrected using Odyssey Infrared Imaging System Application Software Version 3.0 (LI-COR Biosciences) or Evolution-Capt Edge Software Version 18.06 (VILBER Lourmat) and Bio-1D imaging software Version 15.08c (Vilber Lourmat), and protein levels were normalized to GAPDH or β-actin.

427 *qPCR*

428 HepG2 cells were incubated with silymarin (10 µg/ml), silybin (20 µM), or vehicle (ethanol
429 for silymarin, DMSO for silybin) for 24 h. Total RNA of HepG2 cells was isolated with the
430 E.Z.N.A Total RNA Kit (Omega Bio-tek, Norcross, GA). SuperScript III First-Strand
431 Synthesis SuperMix (Thermo Fisher Scientific) was used for transcription into cDNA. The
432 cDNA was snap-frozen and stored at -20 °C until use. An aliquot of the cDNA preparation
433 (1.25 µl) was combined with 1× Maxima SYBR Green/ROX qPCR Master Mix (Fermentas,
434 Darmstadt, Germany) and forward and reverse primer (0.5 µM; TIB MOLBIOL, Berlin,
435 Germany) in Mx3000P 96-well plates. Primer sequences are given in Table 1. β-Actin and
436 GAPDH were used as reference. PCR was performed on a StraTGene Mx 3005P qPCR
437 system (Agilent Technologies, Santa Clara, CA). The PCR program heats to 95°C for 10 min
438 and conducts 45 cycles of 15 s at 95°C, 30 s at 61°C, and 30 s at 72°C. Threshold cycle values
439 were determined by MxPro Software (Mx3005P/version 4.10, Agilent Technologies) and
440 normalized to the amount of total RNA.

441 Table 1. Primer sequences used in real-time quantitative PCR experiments

gene	**sense primer (5‘ → 3‘)**	**anti-sense primer (5‘ → 3‘)**
hGPAT1	GAAGCTGGAGCTGCTGGGCA	AAAGCCACACTCACCCCATTCCT
hGPAT2	TCGTGCTGGGCCAATGTACTG	AGGAGAACTCCCCCAGGAGC
hGPAT3	CTGCCAGACAGCAGCCTCAA	GCCATGAACCTGGCCAACCA
hGPAT4	GCCGCTCAGGATGCACTGG	CCGTGCACTTGACCCACCAT
hLPLAT1/ hLPAAT1	GAGACACAGCCATCCGCCAC	GCAAGATCTTCATGTTCTCGACG TT
hLPLAT2/ hLPAAT2	CGCAACGACAATGGGGACCT	TGCACTGTGACTGTTCCTGAAGT

hLPLAT3/ hLPAAT3	CGGCTGCAGGCTTGTCCA	CAGTTGAGGCGGCGGTGAG
hß-Actin	ACAGAGCCTCGCCTTTGCC	CCATCACGCCCTGGTGCC
hGAPDH	TTTGCGTCGCCAGCCGAG	TTCTCAGCCTTGACGGTGCC

Immunofluorescence microscopy

HepG2 cells (2.5×10^4/3.9 cm^2) were seeded on an ibidi 8-well slide (ibidi #80826, Gräfelfing, Austria) and cultured for 24 h at 37 °C and 5% CO_2. For ER and lipid droplet staining, vehicle (0.1% DMSO for silybin A or 0.05% ethanol for silymarin), silymarin, or silybin were added, and cells were incubated for another 24 h at 37 °C and 5% CO_2. The medium was then removed, and the cells were rinsed twice with HBSS. Prewarmed BioTracker™ 488 Green Lipid Dye Biotracker (Merck, # SCT144, 1x in HBBS /Ca/Mg, Gibco cat. #14025-092) or ER-Tracker™ Red (BODIPY™ TR Glibenclamide) (ThermoFisher Scientific, Vienna, Austria #E34250, 1 µM in HBSS) staining solutions were added and cells incubated for 30-60 min before being washed with HBSS. Hoechst DNA staining solution was applied (Merck, # 33258, 1 µg/ml) and cells incubated for 30 min at 37 °C and 5% CO_2. The staining solution was then removed and the cells were fixed with 4% paraformaldehyde in H_2O for 20 min, followed by two washes with HBSS. Fresh HBSS buffer was added and the cells were immediately visualized by fluorescence microscopy. For Golgi staining, cells were incubated with vehicle (0.1% DMSO for silybin A or 0.05% ethanol for silymarin), silymarin or silybin for 6 h at 37 °C and 5% CO_2. The cells were rinsed twice with HBSS and 2 µL of the BacMam 2.0 reagent CellLight™ Golgi-GFP (ThermoFisher Scientific, Vienna, Austria, # C10591) was added, followed by incubation at 37°C in 5% CO_2 for 18 h. Cells were washed with HBSS twice, Hoechst DNA stain solution was added and cells were incubated for 30 min at 37 °C and 5% CO_2. Fluorescently labelled organelles were visualised using a BZ-X800E

fluorescence microscope (Keyence, Neu-Isenburg, Germany) equipped with the BZ-X Filters DAPI (OP-87762, λ_{ex} = 360 nm, λ_{em} = 460 nm), GFP (OP-87763, λ_{ex} = 470 nm, λ_{em} = 525 nm) and TRITC (OP-87764, λ_{ex} = 545 nm, λ_{em} = 605 nm) and a Plan Apochromat 40× (NA 0.95) objective. Images were captured using the sectioning module with structured illumination and z-stacks of 10 µM. Image analysis was performed using ImageJ software (https://imagej.net/ij/). For quantification of ER and Golgi, a region of interest (ROI) was drawn around the labeled organelles, and the mean intensity was measured. Only cells within the focal plane were considered, defined as cells in which the ER appeared as a perinuclear ring surrounding at least 50% of the nucleus or in which Golgi signals appeared as distinct, well-defined spots. Lipid droplet quantification was performed by setting a minimum threshold of 15 to exclude background staining. Number and size of lipid droplets were automatically measured using the "Analyze Particles" tool in ImageJ.

Immunohistochemistry (IHC)

Liver samples were immediately fixed in neutral buffered 4% paraformaldehyde for at least 24 h and then dehydrated in increasing alcohol concentrations, embedded in paraffin, and sliced into 4 µm sections as described before[87]. The sections were deparaffinized with xylene and rehydrated using an inverse series of aqueous alcohol concentrations. Hydrogen peroxide (0.3% in methanol) was applied for 45 min to block endogenous peroxidase activity. Sections were microwaved in citric acid (10 mM, pH 6.0) for 16 min at 600 W and then incubated with primary antibodies (mouse anti-GRP78, 1:5000; goat anti-rat CYP1A1, 1:5000; goat anti-rat CYP3A2, 1:5000; goat anti-rat CYP2B1, 1:5000) in PBS pH 7.4 and 5% BSA overnight at 4°C, followed by treatment with secondary biotinylated rabbit anti-goat IgG or rabbit anti-mouse IgG (30 min, room temperature) and peroxidase-conjugated avidin (VECTASTAIN® Elite ABC-Kit; Vector Laboratories, Burlingame, CA; another 30 min). The chromogen 3-amino-9-ethylcarbazole (AEC Substrate Pack; BioGenex, San Ramon, CA)

was applied twice for 15 min to visualize immunoreactive sites. Sections were mounted in Vectamount™ mounting medium (Vector Laboratories, Burlingame, CA) and analyzed using an Axio Imager A1 microscope equipped with a 20× objective and a ProgRes C5 camera (Jenoptik, Jena, Germany).

Animal housing and treatment of mice with silybin hemisuccinate

Male C57BL/6 mice (12-weeks-old, body weight 25–30 g; Charles River, Sulzfeld, Germany) were housed under standardized conditions with a day-night cycle of 12 h/12 h at 22 ± 1°C and 50 ± 10% environmental humidity. Standard diet and water were provided *ad libitum*. Animals were adapted to laboratory conditions before the experiment for at least 2 days. Silybin hemisuccinate (200 mg/kg) or vehicle (0.9% NaCl) were intraperitoneally administered trice (at 0, 12, and 24 h). Mice were anesthetized by isoflurane and sacrificed by isoflurane overdose after 37 h, and organs were removed, weighed and either fixed in 10% buffered formaldehyde or snap-frozen in liquid nitrogen for biochemical analysis. All experiments were performed in accordance with the German legislation on protection of animals and with approval of the Thuringian Animal Protection Committee.

GSH and GSSG levels

The tissue content of glutathione in its reduced (GSH) and oxidized (GSSG) form was analyzed by homogenizing the liver and kidney samples with eleven volumes of 0.2 M sodium phosphate buffer (5 mM EDTA; pH 8.0) and four volumes of 25% metaphosphoric acid. After centrifugation (12,000×g, 4°C, 30 min), the GSH content was measured in the supernatants using a colorimetric assay as previously described[88]. The GSSG concentration was assessed fluorometrically[89].

Lipid peroxidation

To determine the tissue content of lipid peroxides as thiobarbituric acid reactive substances (TBARS), liver and kidney samples were homogenized in 19 volumes of ice-cold saline and analyzed fluorometrically[90].

Biotransformation capacity

To obtain 9,000×g supernatants, the livers were homogenized in 0.1 M sodium phosphate buffer (pH 7.4) (1:2 w/v) and subsequently centrifuged at 9,000×g for 20 minutes at 4°C. Activities of all biotransformation reactions were assessed in these 9,000×g supernatants and referred to the protein content of this fraction which was determined with a modified Biuret method[91]. For assessment of CYP enzyme activities, the following model reactions were performed: benzyloxyresurofin-*O*-debenzylation (BROD) [92], ethoxycoumarin-*O*-deethylation (ECOD) [93], ethoxyresorufin-*O*-deethylation (EROD) [94], ethylmorphine-*N*-demethylation (EMND) [95], methoxyresorufin-*O*-demethylation (MROD)[94], pentoxyresorufin-*O*-dependentylation (PROD) [94]. GST activities were determined using *o*-dinitrobenzene as a substrate. The resulting dinitrobenzene-glutathione conjugate was measured photometrically[96]. For the determination of UGT activities, 4-methylumbelliferone was used as a substrate and the respective glucuronide was measured fluorometrically[97,98].

Blood glucose levels

Blood glucose levels were determined using a commercially available blood glucose meter and respective test strips (BG star1, Sanofi-Aventis, Frankfurt, Germany).

Data analysis and statistics

Data are given as individual values and/or means ± SEM or + SEM of *n* independent experiments. Statistical analysis was performed with GraphPad Prism 8.3 or 9.0 (GraphPad

Software Inc, San Diego, CA, USA) using non-transformed or logarithmized data. Ordinary or repeated-measures one-way ANOVAs followed by Tukey *post-hoc* tests were applied for multiple comparison, and two-tailed Student's *t*-tests were used for paired and unpaired observations (two-sided α levels of 0.05). Statistical significance was defined as $*P < 0.05$, $**P < 0.01$, and $***P < 0.001$. Outliers were determined by Grubb's test. Figures were created with Graphpad Prism 8.3 or 9.0 (GraphPad Software Inc), Excel 2016 or 2020 (Microsoft, Redmond, WA), or Sigma Plot 13.0 (Systate Software GmbH, San Jose, CA).

Results

Silybin induces a switch from hepatic TGs to phospholipids

To investigate the effects of silymarin and silybin on the hepatic lipid composition, we monitored concentration- and time-dependent changes in PE levels in HepG2 cells by targeted lipidomics. Phospholipid accumulation in HepG2 cells was manifested at ≥ 10 µg/ml silymarin or 20 µM silybin after 24 h (Figure S1), and cytotoxic activities first became evident at ≥ 50-200 µg/ml silymarin and ≥ 100 µM silybin (Figure S2). For the following experiments, human HepG2 hepatocarcinoma cells and human primary monocytes (as a surrogate for hepatic phagocytes) were used and treated with 50 µg/ml silymarin for monocytes, 10 µg/ml silymarin for HepG2 cells and 20 µM silybin for 24 h. Silymarin increased the cellular content of major phospholipid classes, i.e., PC, PE, phosphatidylserine (PS), phosphatidylinositol (PI), phosphatidylglycerol (PG), and SM (Figure 1B and C). Similar effects were observed for silybin (20 µM, Figure 1B and C), one of the major bioactive components of silymarin [43]. Instead, TG levels were substantially decreased by both silymarin and silybin treatment, with opposite efficacy in monocytes and hepatocytes. While silymarin specifically reduced TG levels in monocytes, silybin was only effective in hepatocytes (Figure 1B and C). Together, our results suggest that silybin induces a hepatic

558 switch from TGs to phospholipids and point to additional components contained in silymarin
559 that tune the cellular lipid profile.

560 To investigate whether the decrease in TGs is functionally related to the accumulation of
561 phospholipids, we studied the impact of TG degradation on the cellular PE content, which
562 was robustly upregulated by silybin treatment (Figure 1C). The selective diacylglycerol-*O*-
563 acyltransferase (DGAT)2 inhibitor PF-06424439 (10 μM), which interferes with the final step
564 of TG biosynthesis [99], decreased TG levels as expected, but failed to increase the amount of
565 PE (Figure S3). Accordingly, inhibition of adipocyte triglyceride lipase (ATGL) using
566 atglistatin neither decreased TG nor significantly elevated PE levels (Figure S3). Thus, our
567 data suggest that the reduction in TGs does not account for the enrichment in phospholipids,
568 at least under conditions where phospholipid biosynthesis is not upregulated.

569 Next, we investigated whether silybin counter-regulates phospholipid and TG levels *in vivo*.
570 Mice received silybin (200 mg/kg, i.p.) three times over 37 h, which is expected to produce
571 peak hepatic concentrations >10 nmol/g for the unconjugated drug [100,101]. Silybin
572 increased the hepatic phospholipid content, reaching significance for PE, PS, and PI, and
573 simultaneously lowered TG levels (Figure 1D), as expected from the results for hepatocytes *in*
574 *vitro*. The shift from TGs to phospholipids was accompanied by a significant loss of liver and
575 body weight (Figure 1E) and a decrease of blood glucose levels (Figure S4), which is of
576 particular interest because fatty liver disease is often associated with insulin resistance that
577 elevates blood glucose levels [3]. Note that the mice were fed ad libitum and food intake was
578 not measured. Therefore, it cannot be excluded that the observed effects of silybin may be
579 partially related to reduced food intake.

580 The majority of phospholipids significantly upregulated by silybin in mouse liver contain
581 polyunsaturated fatty acids, either linoleic acid (18:2), arachidonic acid (20:4), or
582 docosahexaenoic acid (22:6) (Figure 2A). Note that an increase in membrane unsaturation has

583 been associated with insulin sensitivity [102] and may explain the decrease in blood glucose
584 levels with silybin administration (Figure S4). The effect of silymarin/silybin on individual
585 lipid species varies greatly between experimental systems (Figure S5 and S6). While the
586 levels of a broad spectrum of phospholipid species are increased, there are also lipids that are
587 regulated in the opposite direction, particularly in mouse liver, where silybin reduces the
588 amount of PC(18:1/18:1) and PE(18:1/18:1), along with other lipids (Figure 2A and Figure
589 S6). The differences between silymarin and silybin lie in the magnitude rather than the
590 direction of the phospholipidomic changes (Figure 2B). In contrast, the levels of TG species
591 are consistently decreased by silymarin in monocytes and by silybin in HepG2 cells (Figure
592 S5). To exclude that lipids present in silymarin contribute to changes in the cellular lipid
593 profile, we analyzed the lipid composition of silymarin. Phospholipids with a glycerol
594 backbone (glycerophospholipids) other than PC(16:0/18:2) were not detected in silymarin,
595 and only low-abundance lysophospholipid and SM species were present (Figure S7).
596 Together, the lipids in silymarin do not explain the increase in cellular phospholipids upon
597 treatment.

598

599 ***Accumulated phospholipids are distributed across intracellular membranes***

600 Phospholipids are organized in plasma and intracellular membranes and, to a lesser extent, in
601 lipid droplets and the cytosol [13,103]. It can be excluded that the silymarin/silybin-induced
602 increase in cellular phospholipids is related to the plasma membrane, as the diameter of both
603 monocytes and HepG2 cells was not altered by treatment (Figure S8A). To define the
604 membrane compartment where the additional phospholipids are deposited, we assessed their
605 size and morphology using organelle-specific fluorescence probes (Figure S8). We expected
606 that the 1.2- to 1.5-fold increase in total intracellular phospholipids would be visible as a gain
607 in size or morphological change if the additional phospholipids were preferentially

608 incorporated into a specific membrane compartment. If, instead, the phospholipids are evenly
609 distributed throughout the intracellular membranes, even the 1.5-fold increase in spherical
610 surface area (formed by membrane phospholipids) would result in only a 1.2-fold increase in
611 diameter, and this factor is further reduced for tubular systems such as ER and Golgi with
612 strongly increased surface areas as compared to spherical structures. Apparent effects on
613 organelle size and structure (as assessed by quantitative analysis of the fluorescence probes)
614 are unlikely to be achieved in this case. We focused on large intracellular membrane
615 compartments, i.e., nucleus, ER, and Golgi, which were stained with Hoechst DNA stain and
616 live cell dyes for ER and Golgi, respectively. Silymarin/silybin A did not markedly affect the
617 intensity or distribution of the fluorescence signal (Figure S8B and C), as confirmed by
618 quantitative analysis of the fluorescence signal (Figure S8B and C). Thus, phospholipids seem
619 to be enriched at intracellular sites but not preferentially incorporated into a major membrane
620 compartment such as the ER, Golgi, or nucleus.

621

622 ***Silybin causes a decrease in lipid content***

623 Lipid droplets are universal storage organelles for neutral lipids such as TG and cholesteryl
624 esters (CE) and represent dynamic cellular organelles with an important role in lipid and
625 membrane homeostasis [13]. We treated HepG2 cells with silymarin or silybin (A) and
626 stained lipid droplets with either Oil Red O or BioTracker™ 488 Green Lipid Dye.
627 Spectroscopic analysis of lipid droplets, quantifying the incorporated Oil Red O (Figure S8E),
628 showed that silybin reduced their content. Interestingly, this reduction was not due to a
629 decrease in the number of lipid droplets, but rather appeared to result from a decrease in their
630 size (based on image quantification of cells stained with the BioTracker Lipid Dye) (Figure
631 S8D). These findings are consistent with the observed decrease in TG levels (Figure 1C) as
632 well as with previous *in vitro* and *in vivo* studies using silymarin or silybin [104-108].

633 Silymarin was considerably less efficient in reducing TG levels (Figure 1C), and lipid droplet
634 content in HepG2 cells (Figure S8D and E).

635

636 ***Stereochemical requirements of silybin for targeting lipid metabolism***

637 Natural silybin is a mixture of the diastereoisomers silybin A and B [43]. To elucidate the
638 active isomer and explore crucial structural features, we applied an efficient preparative
639 HPLC method to obtain the two isomers A and B in pure form [65]. Starting from these
640 isomers, the corresponding 2,3-dehydrosilybin enantiomers and the hemiacetal product, in
641 which the 2,3-dihydro-chromane is replaced by 2*H*-benzofuran-3-one, were synthesized [66]
642 (Figure 3). Lipidomic analysis revealed that silybin A increased phospholipid and decreased
643 TG levels in HepG2 cells, whereas silybin B was considerably less effective (Figure 3).
644 Introduction of a double bond into the flavanon-3-ol moiety of silybin yielded 2,3-
645 dehydrosilybin, which (as *7'R,8'R* isomer A) decreased TG levels comparably to silybin but
646 was no longer active on phospholipids (Figure 3). These findings indicate that both, the 2,3-
647 dihydrochromane and the 1,4-benzodioxan scaffold of silybin A contribute to the
648 phospholipid-accumulating activity, whereas modifications of the 2,3-dihydrochromane ring
649 are compatible with TG-lowering properties. Hence, silybin seems to modulate TG and
650 phospholipid metabolism through independent mechanisms. 2,3-Dehydrosilybin and its
651 isomers A and B (Figure 3) selectively decreased the abundance of anionic phospholipids. On
652 the one hand, 2,3-dehydrosilybin lowered the cellular PS content, which we ascribed to
653 isomer B. On the other hand, both isomers, but surprisingly not the stereomeric mixture,
654 induced a drop of PG (2,3-dehydrosilybin A > 2,3-dehydrosilybin B), the precursor of
655 cardiolipins [64]. The hemiacetal (Figure 3) increased phospholipid and decreased TG levels
656 by trend, being slightly less efficient than silybin A (Figure 3**)** but more active than the
657 stereomeric mixture of silybin (Figure 1C). Neither cell number nor membrane integrity were

substantially reduced by any of the silybin derivatives up to 20 µM (Figure S9). Together, the effects of silybin on the cellular lipid profile are mediated by only one isomer, and small changes in its structure allow to dissect the activities on phospholipids and TGs.

Silymarin/silybin acts on multiple nodes in the lipid metabolic network, reducing the overall expression of enzymes involved in triglyceride biosynthesis and phospholipid degradation

To elucidate the molecular mechanisms by which silymarin/silybin induces a lipid class switch from TGs to phospholipids, we reanalyzed previously published transcriptomic datasets from hepatocytes (*in vitro* and *in vivo*) and acquired the transcriptome of an exemplary extrahepatic cell line to distinguish liver-specific from general effects. We focused on genes from the category "Lipid Metabolism" of the Reactome Pathway Database [109] and studied their expression in four experimental systems *in vitro* and *in vivo*: i) human HepG2 hepatocarcinoma cells treated with silymarin (12 µg/ml) for 24 h [83], ii) human Huh7.5.1 hepatocarcinoma cells treated with silymarin (40 µg/ml) for 4, 8, and 24 h [84], iii) human Caco-2 colon carcinoma cells treated with either silybin (30 µM) or silymarin (30 µg/ml) for 24 h, and iv) hepatocytes isolated from chronically hepatitis C virus (HCV)-infected mice receiving daily intravenous injections of silybin (265-469 mg/kg) for 3 or 14 d [85]. Silybin/silymarin affects the expression of a wide range of enzymes and factors involved in lipid metabolism, but the effects are moderate and, with one exception, do not reach significance after global correction for false discovery (Figure S10A-D). Only the cytochrome P_{450} (CYP) monooxygenase *CYP1A1*, which accepts various endogenous substrates, including steroids and polyunsaturated fatty acids [110-114], is highly significantly upregulated in Caco-2 cells (Figure S10C).

682

683 ***Silymarin/silybin induces the expression of enzymes involved in phospholipid biosynthesis,***
684 ***while reducing the expression of phospholipid degradation enzymes***

685 Given the detected changes in the HepG2 lipidome (Figure 1B-D), we extended our study to
686 genes that were differentially regulated according to non-adjusted *P*-values and for which the
687 respective pathway was significantly regulated in the same direction for at least two
688 independent model systems. We found that silybin/silymarin i) decreased the expression of
689 several lipases involved in phospholipid degradation (Figure 4A-F), including phospholipases
690 A_1 (*PLA1A*, Figure 4B), phospholipases A_2 (*PLA2G1B, PLA2G6*, Figure 4A and D, and
691 Figure S11), and phospholipase D (*PLD1, PLD6*, Figure 4A, B, and D, and Figure 11),
692 specifically in primary hepatocytes and hepatocyte-derived cell lines.

693 In addition, silybin/silymarin ii) upregulates factors that deplete phospholipases (*PLA2R1*,
694 Figure 4B), iii) downregulates enzymes that degrade intermediates in phospholipid
695 biosynthesis (*TECR, MGLL, ACP6, GDPD3, PNPLA7*, Figure 4B, D and E), and iv) less
696 consistently induces the expression of phospholipid biosynthetic enzymes and other factors
697 (*GNPAT, CHKA, SLC44A1, AGPS, AGPAT2, MBOAT2, LPGAT1, DEGS1, CERS6*, Figure
698 4C and D and Figure S11).

699 Compensatory mechanisms seem to exist that decrease phospholipid biosynthesis (*via*
700 *PCYT1A, ETNK2, PEMT, GPAM, SPTLC3, CERS2*, Figure 4B, C, D and E) or enhance
701 phospholipid degradation (*PLA2G4C, DDHD1, ACER3, PLD6*, Figure 4B, C and D), possibly
702 buffering the accumulation of phospholipids or rearranging phospholipid profiles through
703 different substrate specificities.

704 To investigate whether silymarin/silybin elevates phospholipid levels *via de novo*
705 phospholipid biosynthesis under our experimental conditions, we treated HepG2 cells with

706 silymarin or silybin for 24 h and determined the mRNA expression of glycerophosphate
707 acyltransferase (*GPAT*) isoenzymes and lysophosphatidic acid acyltransferase
708 (*LPAAT*)/lysophospholipid acyltransferase (*LPLAT*) isoenzymes at the mRNA level. *GPATs*
709 and *LPAATs* successively transfer acyl-chains from acyl-CoA to the *sn*-1 and *sn*-2 positions
710 of glycerol-3-phosphate to form phosphatidic acid, the common precursor of
711 glycerophospholipids and TGs [64]. Silymarin and silybin increased the mRNA levels of
712 *GPAT* isoenzymes 2 to 4, reaching significance for the silymarin-mediated induction of
713 *GPAT3* (Figure 4G), which is consistent with a previous report showing enhanced *Gpat3*
714 mRNA expression in the liver of silybin-treated mice on a methionine- and choline-deficient
715 diet [104]. In contrast, the expression of *LPAAT*/*LPLAT* isoenzymes was not markedly
716 affected (Figure S12A). Together, the moderate but versatile induction of phospholipid
717 biosynthesis and inhibition of phospholipid degradation by silymarin/silybin likely accounts
718 for the accumulation of phospholipids in hepatocytes.

719

720 ***Silymarin/silybin reduces the expression of triglyceride-synthesizing enzymes***

721 The decrease in TG levels is driven by the repression of genes associated with the generation
722 of DAGs from either phosphatidate (*LPIN2, LPIN3, PLPP1, PLPP3*, Figure 4A and C, and
723 Figure S11) or monoacylglycerols (*MOGAT2*, Figure 4E) and their acylation to TGs (*DGAT1,*
724 *DGAT2*, Figure 4A, B, C and E, and Figure S11), as suggested by comparative
725 transcriptomics. The concrete mode of action seems to be context-dependent and possibly
726 under kinetic control, as suggested by the failure of silybin and silymarin to reduce DGAT1
727 and DGAT2 protein expression in HepG2 cells 24 h after treatment (Figure S12B). TGs are a
728 major component of the hydrophobic core of lipid droplets, which form contact sites with
729 essentially all other cellular organelles and are at the nexus of lipid and energy metabolism
730 [13,115,116]. Interestingly, selective inhibition of DGAT1 (by A-922500) or DGAT2 (by PF-

06424439) and antagonism of the DGAT-inducing transcription factor peroxisome proliferator activated receptor (PPARγ) [117] (by GW9662) moderately reduced lipid droplet staining in palmitate (PA, 16:0)-loaded human HepaRG hepatocytes (Figure 5A), but only the combined inhibition of DGAT1 and DGAT2 reached the efficacy of the silybin isomer A (Figure 5B). Since lipolysis of TGs in lipid droplets is initiated by ATGL/PNPLA2 [118], we investigated the effect of silymarin/silybin on the protein expression of this enzyme, but again found no substantial regulation (Figure S12B), consistent with the transcriptomics data (Figure 4A-E). Note that selective inhibition of ATGL (by atglistatin) also failed to increase lipid droplet signals in stressed HepaRG cells (Figure 5A).

Silymarin/silybin causes subtle changes in fatty acid anabolism

Both phospholipid and TG biosynthesis depend on the availability of activated fatty acids [119]. Their biosynthesis from acetyl-CoA is an energy- and NADPH-consuming process, which is initiated by the rate-limiting enzyme acetyl-CoA carboxylase (ACC, *ACACA*) [120]. The product of this reaction, malonyl-CoA, is subsequently transferred to fatty acid synthase (*FASN*), which produces long-chain fatty acids that are activated as CoA esters by acyl-CoA synthetases before further metabolism [121,122]. As expected from the multiple roles of acyl-CoAs in lipogenesis, silymarin/silybin ambiguously regulates genes related to fatty acid metabolism, with expression changes either promoting or inhibiting *de novo* fatty acid biogenesis (*ACACA, FASN, SCD5,* Figure 4A, C, and E), fatty acid uptake respectively activation (*SLC27A1, SLC27A2, SLC27A5, ACSL4, ACSL6,* Figure 4A, D, E), fatty acid elongation (*ELOVL4, ELOVL6, ELOVL7, TECR,* Figure 4B, D and E), and the intracellular transport of acyl-CoAs (*ACBD4, DBI, HACD1,* Figure 4B, C and E). In HepG2 cells, silymarin/silybin slightly increased ACC/*ACACA* (but not FASN) protein expression, which was significant for silybin (Figure S12B), while ACC phosphorylation, which inactivates

ACC [120], tend to be decreased (Figure S12B). This weak stimulatory regulation of ACC by silymarin/silybin was not translated into increased cellular concentrations of i) malonyl-CoA (ACC product, Figure S12C), ii) long-chain fatty acids (FASN products, Figure S12C), or iii) long-chain acyl-CoAs (acyl-CoA synthetase products, Figure S12C). Conclusively, silybin and silymarin induce changes in fatty acid anabolism that may contribute to, but do not appear to be essential for, the lipid class switch from TGs to phospholipids.

Silymarin/silybin A promotes phospholipid biosynthesis

To evaluate the effects of silymarin and silybin A on the biosynthesis of phospholipids and TGs, we treated HepG2 cells with silymarin or silybin A for 6 h and supplied them with $^{13}C_2$, d_3-labelled sodium acetate for additional 18 h. Newly synthesized PE and TG species were detected as M+3 signals by UPLC-MS/MS, with corrections applied for naturally occurring isotopes. As expected, both silymarin and silybin A significantly increased the incorporation of isotopically labelled acetate into PE species, particularly in PE(16:0_18:1) with M+3 in 16:0, PE(18:_18:1) with M+3 in 18:0, and PE(18:0_18:1) with M+3 in 18:1 (Figure 4I and Figure S13A and C). Note that silymarin also led to a significant incorporation of labled acetate (M+3) into TG species (Figure 4J and Figure S13C and D) and that silybin A displayed a similar trend (Figure 4J and Figure S13C and D). These findings suggest that both silymarin and silybin A stimulate lipid biosynthesis, with silybin A showing a particular preference for phospholipids. Given that silybin, but not silymarin, reduces TG levels (Figure 1B, C), our data strongly suggests that silybin preferentially acts at the level of TG degradation and/or lipid droplet remodeling, an effect that may be compensated for silymarin by the stronger stimulatory effect on TG biosynthesis (Figure 4J).

Silymarin but not silybin enhances fatty acid degradation for specific settings

Since the intracellular concentration of long-chain fatty acids is not markedly altered by silymarin/silybin (Figure S12C), while the fatty acid storage capacity in TGs is compromised (Figure 1B-D), we addressed the fate of fatty acids. On the one hand, they seem to be channeled towards phospholipid biosynthesis, as supported by our data (Figure 1B-D). On the other hand, they might be subjected to fatty acid oxidation *via* mitochondrial or peroxisomal pathways to sustain the energy demand for phospholipid biosynthesis [32,123-125]. In support of this hypothesis, oral administration of silybin increased the mRNA expression of carnitine palmitoyl-transferase 1α (*Cpt1a*) in mouse liver, suggesting an efficient transfer of acyl-CoAs into mitochondria for β-oxidation [104]. Transcriptomic analysis underlines that mitochondrial (*HADH, ACAT1, ACADVL*, Figure 4C, Figure S11) and peroxisomal β-oxidation (*ACOX3, HAO2*, Figure 4A) are enhanced for specific settings, and we confirmed in cultured HepG2 cells that silymarin increased the levels of the β-oxidation intermediate butyryl-CoA in cultured hepatocytes (Figure 4H). However, the effect does not seem to be mediated by silybin, which failed to enrich β-oxidation intermediates (Figure 4H). Since extensive fatty acid oxidation depletes fatty acid concentrations and thus competes with efficient phospholipid biosynthesis, we would expect fatty acid degradation to be kept in check. Consistent with these considerations, silymarin/silybin decreased the mitochondrial degradation of straight-chain, odd-chain, and branched fatty acids (*CPT2, ACAA1, ACAA2, HADH, ACADS, HADHB, PCCA, MCEE,* Figure 4B, C, D, E, Figure S11) as well as peroxisomal oxidation (*ABCD1, ACOX2, PHYH*, Figure 4C and E, Figure S11) and ketogenesis (*HMGCS2, BDH1, HMGCLL1,* Figure 4B, C, E), especially in mouse liver *in vivo* and Huh7.5.1 hepatoma cells *in vitro*. Fatty acid oxidation by CYP enzymes is also subject to intense regulation. Among the various CYP enzymes repressed by silymarin/silybin are those involved in the epoxidation and hydroxylation of polyunsaturated fatty acids

(*CYP2C8, CYP2C9, CYP2C19, CYP3A4*, Figure 4E, Figure S11). ω-Oxidases are instead upregulated (*CYP4F2, CYP4A22*, Figure 4B and Figure S11), and results for *CYP1A1* are mixed (Figure 4B, C and E).

A detailed description of the impact of silymarin/silybin on cholesterol and CE metabolism is given in Supplementary Note 1.

Together, silymarin/silybin induce a lipid class switch from TGs to phospholipids by interfering with lipid metabolism at multiple nodes rather than strongly regulating a single specific target. Most importantly, silymarin/silybin limits TG biosynthesis and suppresses phospholipid degradation in both hepatocytes and extrahepatic cells, partly combined with enhanced phospholipid biosynthesis. These central adaptations are accompanied by pronounced changes in cholesterol and fatty acid metabolism.

Efficacy of silybin in in vitro models of MAFLD and lipotoxicity

The predominant fatty acids present in TGs of the liver, both in healthy individuals and in MAFLD patients, are palmitic acid (PA, 16:0) and oleic acid (OA, 18:1) [126]. Following previously published procedures [127], we established *in vitro* models of MAFLD and acute lipotoxicity by overloading human HepaRG cells (as a surrogate for normal hepatocytes [128]) with a balanced saturated/unsaturated fatty acid mixture (PA:OA = 1:2) or by challenging them with the saturated fatty acid PA [127]. We monitored the (time-dependent) increase in lipid droplets (Figure 5B and Figure S14A), TG levels (Figure 5C and Figure S14B), and phospholipid content, specifically PE (Figure 5D and Figure S14C) and PC levels (Figure S14D), and determined the consequences on cellular dehydrogenase activity (as a measure of cell viability) (Figure 5E and Figure S14E), viable cell number (Figure S14F), and membrane integrity (Figure S14G). PA/OA strongly increased lipid droplet staining (Figure

827 5B), elevated TG levels (Figure 5C), and caused a shift from PE (Figure 5D) to PC (Figure
828 S14D) within 24 h. PA was less efficient in increasing TG levels and did not enhance the lipid
829 droplet signal (Figure 5B), but raised the levels of both phospholipid subclasses investigated
830 (Figure 5D, C and Figure S14D), as expected from the associated induction of ER stress and
831 the UPR [129,130]. The effects were less pronounced or even disappeared at longer
832 incubation times (48 h) (Figure S14A-D). While OA/PA did not or hardly impair the
833 metabolic activity of the cells (Figure 5E and Figure S14E), PA was cytotoxic within 24 h
834 (EC_{50} = 70 μM) (Figure 5E, and Figure S14E), but did not yet disrupt membrane integrity
835 (Figure S14G) or reduce the number of viable cells (Figure S14F).

836 To further validate the experimental model, we first investigated whether silybin A is able to
837 induce a lipid class switch in unchallenged HepaRG cells, as expected from our studies in
838 HepG2 cells (Figure 3). Indeed, silybin A (although the effects were less pronounced)
839 induced a lipid class switch in HepaRG cells, but apparently from neutral lipids in lipid
840 droplets to phospholipids (Figure 5B and Figure S14D), with little effect on total cellular TG
841 levels (Figure 5C). We then investigated the effect of silybin A in the two disease models (PA
842 or PA/OA treatment): silybin A still reduced the lipid droplet (but not TG) content (Figure 5B
843 and C), but became less efficient in upregulating phospholipid levels (Figure 5D, and Figure
844 S14C and D) and did not attenuate the lipotoxic drop in cell viability (Figure 5E). Our data
845 indicate that silybin A preferentially redirects lipid metabolism from TGs to phospholipids in
846 healthy hepatocytes and extrahepatic cells, and that this metabolic switch becomes less
847 efficient under severe lipid overload, which might provide a mechanistic basis for the mixed
848 results in clinical trials both, under disease and non-disease conditions [131-136].

849

Activation of hepatic phase I and II metabolism in healthy mice

Silybin induces the expression of phase II enzymes (including glutathione S-transferase, GST) in mouse liver and other tissues [101,137-139]. Instead, the consequences on CYP monooxygenases (phase I enzymes) are mixed [101,139-141], possibly due to superimposed direct enzyme inhibition, differences between healthy and diseased states, and different kinetics [142-145]. To gain an overview about the global regulation of drug-metabolizing enzymes by silymarin/silybin, we analyzed the transcriptome data from the experimental systems described in section "*Silymarin/silybin acts on multiple nodes in the lipid metabolic network*" for changes in the expression of genes of the Reactome Pathway Database [109] categories 'metabolism - oxidation', 'phase I metabolism (compound functionalization)', and 'phase II metabolism (compound conjugation)'. Hepatocytes from silybin-treated HCV-infected mice showed a clear kinetic trend: genes of drug-metabolizing enzymes are initially upregulated (day 3) and then downregulated with prolonged treatment (day 14) (Figure 6A). Instead, the mRNA expression of *CYP* enzymes was differentially regulated in cell-based systems, with individual isoenzymes being up- or downregulated (Figure S15A-C), following independent kinetics (Figure S15B). With few exceptions (*CYP3A5, CYP26A1*, Figure 6A and B, Figure S15B), silymarin/silybin decreased the mRNA expression of those CYP enzymes that are prominently involved in drug metabolism (*CYP2B6, CYP2C8, CYP2C9, CYP2C19, CYP3A4*, Figure 6A and B, Figure S15B and D) and of amino oxidases (*AOC3, MAOA, MAOB*) (Figure 6A and B, Figure S15A and B), which oxidatively deaminate xenobiotic amines, in cell-based systems and *in vivo* after prolonged administration. Based on these data, we speculated that, in healthy mice receiving silybin for a short period of time (24 h), the increase in intracellular membranes is functionally coupled to membrane protein biosynthesis and accompanied by an increased availability of membrane-bound phase I and II isoenzymes that metabolize and detoxify xenobiotics [146,147]. In fact, the protein levels of CYP3A2 and

875 CYP2B1 (but not CYP1A1) were markedly enhanced in the liver of mice receiving silybin
876 hemisuccinate, as shown by immunoblotting (Figure 6C and S16A) and visibly confirmed for
877 all CYP isoforms tested by immunohistochemical analysis (Figure 6D). By contrast, the total
878 amount of hepatic proteins decreased (Figure S16B). CYP enzyme expression was mainly
879 concentrated around the endothelial cells of the central veins. Accordingly, the
880 biotransformation activity of CYP enzymes (Figure 6E), GST and UDP-
881 glucuronosyltransferase (UGT) increased strongly (Figure 6F), as determined by the
882 conversion of indicative substrates, possibly to support silymarin glucuronidation and
883 excretion [36]. Likely as a consequence of the increased GST turnover, the hepatic
884 glutathione (GSH) pool decreased, with both GSH levels and the ratio to glutathione disulfide
885 (GSSG) being significantly reduced (Figure 6G and H**)**. Since GSH, as an essential co-
886 substrate of glutathione peroxidase (GPX)4, contributes to the reduction of lipid
887 hydroperoxides and prevents degenerative cell death [148], we speculated that the decrease in
888 GSH might enhance lipid peroxidation, which was, however, not the case (Figure 6I). Silybin
889 actually attenuated the formation of lipid peroxidation products by trend in the liver but not in
890 the kidney (Figure 6I), consistent with previous studies on silymarin/silybin [105,149,150].

891 Together, the silybin-mediated accumulation of hepatic phospholipids (Figure 1B-D) is
892 associated with an upregulation of membrane-bound detoxifying enzymes as well as GST
893 isoenzymes that are present in different subcellular membrane compartments, including
894 cytosol, mitochondria, ER, plasma membrane and nucleus [151].

895 For information on the effects of silymarin/silybin on vitamin A metabolism, see
896 Supplementary Note 2.

897

Discussion

The efficacy of silymarin and its major active component, silybin, in alleviating toxic liver injury and metabolic diseases [51] has been ascribed to hepatoprotective, anti-inflammatory, anti-oxidative response-inducing and membrane-stabilizing properties as well as to lipid-(TG and cholesterol)-lowering effects [38,152,153]. Here, we report that silybin induces a metabolic switch in hepatocytes and extrahepatic cells, especially under non- or pre-disease conditions, linking hepatic TG metabolism with membrane biogenesis and potentially biotransformation activity (Figure 7), with the latter potentially contributing to the liver protective function.

Effects of silymarin/silybin on lipid-metabolizing enzymes

Specifically, silybin treatment lowers TG levels, while limiting phospholipid degradation in hepatocytes and, under certain settings, additionally stimulates phospholipid biosynthesis, reflecting a net transfer of fatty acids from TGs to phospholipids (Figure 7). Context-dependent adaptations of fatty acid biosynthesis, intracellular transport, mitochondrial and peroxisomal degradation, cholesterol biosynthesis, and sterol metabolism further add to the class switch from TGs to phospholipids. Consequently, the size of lipid droplet decreases while the content of membrane phospholipids increases. At the same time, intracellular membranes are formed that, when coordinated with an upregulation of phase I and II membrane-(associated) enzymes, may enhance the biotransformation capacity of subcellular compartments, such as the ER. A decrease of hepatic lipid droplet size and TG levels is generally considered beneficial in metabolic diseases [10,154]. In support of this principle, increased ATGL/PNPLA2 expression protects against hepatic steatosis [155], whereas ATGL/PNPLA2 repression promotes the development of MAFLD [156,157]. On the other hand, lipolysis is also associated with elevated levels of free fatty acids, which in excess may be lipotoxic to hepatocytes or cause oxidative stress when being degraded by mitochondrial or

peroxisomal β-oxidation [6,158]. Thus, suppression of TG biosynthesis by selective inhibition of DGAT2 improves steatohepatitis and insulin sensitivity, but at the same time exacerbates liver damage in a methionine and choline deficient (MCD) mouse model of NASH [6]. However, in alternative animal models (such as those using diets high in fructose, saturated fat, and cholesterol [159], or Western diets [160]), DGAT2 inhibition reduced steatosis without affecting inflammation or fibrosis in the latter. Conclusively, the reduction of lipid droplets and TGs alone does not fully explain the hepatoprotective function of silymarin and silybin, but requires an efficient channeling of the degradation products into non-toxic metabolites, i.e., phospholipids, as suggested by our results. A similar redistribution was observed for the inhibition of DGAT2 (PF-06424439), although it was restricted to the ER and PE species [161]. This metabolic switch to phospholipids is likely to be of biomedical relevance in toxic liver injury and MAFLD/MASH, where either the hepatic content of total phospholipids or specific phospholipid subclasses is decreased [35,53,54,62]. Consistent with this metabolic dysregulation, many key regulatory factors of MAFLD involve enzymes that are central to phospholipid and TG metabolism, including PNPLA3 [30], LPIAT1/MBOAT7 [19,29,30,131,162], ATGL/PNPLA2 [22], iPLA2/PLA2G6 [23,24], PLA2G7 [163], PLA2 activity of PRDX6 [27], PLD1 [28], and LPIN2 [21]. Altogether, genetic variations or changes in protein expression of these enzymes define the risk of developing MAFLD [20,164] and, together with other regulatory mechanisms, may shape the aberrant lipid composition of the diseased liver, with decreasing phospholipids and increasing TGs [32-35,165-167]. Silymarin/silybin regulates a significant number of these lipid metabolic genes, including *iPLA2/PLA2G6*, *ATGL/PNPLA2, PLD1*, *LPIN2*, and by trend *PNPLA3* (which is a major genetic risk factor for MAFLD [131]) and *HSD17B13*, counteracting the observed dysregulation in liver diseases. In line with our findings, a recently published randomized controlled trial showed that silybin treatment improved MAFLD parameters only in patients

948 without a genetic predisposition, while it was ineffective in patients carrying either one or a
949 combination of mutations responsible for genetically inherited forms of MAFLD [131]. Given
950 that the metabolic and genetic components of MAFLD differ fundamentally [168], these
951 findings suggest that silymarin/silybin may be particularly effective against the metabolic, but
952 not against the genetic, form of MAFLD.

953 In addition, we show here that silymarin/silybin represses the potentially disease-promoting
954 oxidative metabolism of fatty acids (via mitochondrial and peroxisomal pathways but also
955 CYP enzymes) in many settings, including primary mouse hepatocytes, although opposite
956 regulations were also observed at the transcriptome level.

957 Diverse mechanisms have been discussed for the TG- and cholesterol-lowering activity of
958 silymarin/silybin: i) reduced lipid resorption, ii) upregulated cholesterol efflux *via* (ABC)
959 transporters that excrete cholesterol from the liver to the bile [104,152,169], and iii)
960 adjustments in lipid biosynthesis, transport, and degradation by targeting major transcription
961 factors in lipid metabolism [58,61,104,170-172], such as PPARα/PPARγ, LXR; ChREBP and
962 SREBP-1c [55,171-174]. Lipid-metabolic proteins proposed to be affected by
963 silymarin/silybin include enzymes involved in fatty acid biosynthesis (ACC/*ACACA*, FASN,
964 SCD-1), uptake (FABP5), and degradation (CPT1α, ACOX), phospholipid biosynthesis
965 (GPATs), lipid transport (MTTP), and phosphatidic acid/TG turnover (PNPLA3)
966 [58,61,104,170-172,175]. While these studies focused on the ability of silymarin/silybin to
967 restore expression levels under pathophysiological conditions, we first addressed non-stressed
968 cells, healthy mice, and pre-disease conditions. Comparative transcriptomic analyses in four
969 different model systems confirmed that silymarin/silybin differentially regulates pathways
970 contributing to TG and phospholipid metabolism. Specifically, our analysis revealed that
971 silybin broadly manipulates phospholipid metabolism, although the exact mechanism varies
972 between model systems and experimental settings. Overall, we show that silymarin/silybin

973 reduces phospholipid degradation by repressing various phospholipases (*PLA2G1B*, *PLA2G6*,
974 *PLD1,* and/or *PLD6*) or inducing the expression of phospholipase-suppressing factors (e.g.,
975 *PLA2R1*). However, the specific enzymes targeted can vary between different experimental
976 models, and in some cases alternative enzymes may be upregulated, potentially acting as
977 compensatory mechanisms. Less consistently, silymarin/silybin also upregulates the
978 expression of factors involved in acyl-CoA supply (e.g., *FASN*, *SLC27A1, ELOVL7, ACSL4)*
979 and phospholipid biosynthesis (e.g., *MBOAT2*, *LPGAT1*), *via* both *de novo* and remodeling
980 pathways. In support of the relevance of this mechanism, we show that silymarin and silybin
981 increase the incorporation of isotopically labeled acetate into phospholipids. On the other
982 hand, silymarin/silybin seems to suppress TG biosynthesis in several experimental systems,
983 mainly by repressing enzymes involved in the generation of DAGs and their acylation to TGs
984 (e.g. via DGAT1 and DGAT2). In HepG2 cells, DGAT1/2 protein expression was not
985 repressed by either silybin or silymarin (at least under our experimental conditions), allowing
986 us to determine independent effects on the rate of TG biosynthesis, which actually increased,
987 especially for silymarin. These data suggest that silymarin/silybin rather than suppressing TG
988 biosynthesis regulates TG remodeling in HepG2 cells, as supported by the observed decrease
989 in lipid droplet size. The situation may be different in other experimental systems, in which
990 suppressive effects on TG biosynthesis are expected based on transcriptome analysis.

991 The important role of silymarin/silybin in modulating lipid metabolism has been recognized
992 before, and effects on ACC [55,108,176], FASN [55,108,169,172,176-178], SCD-1
993 [14,104,172,179], GPATs [104], PNPLA3 [104,175,177] , FABP5 [104,172,179], CPT1a
994 [55,104,108,172,178,180], MTTP [104], ACOX [104], PPARα/PPARγ
995 [55,104,172,173,175,177,180,181] and SREBP-1c [55,104,175-177,180,181] have been
996 reported independently, either under disease [55,60,61,104,150,171,175,176,182] or non-
997 disease conditions [58,169,177,178], largely without considering their interplay. By

converging transcriptomics, metabololipidomics, and functional studies, we put these individual findings into context. Thus, our data strongly suggest that silybin, by coordinating multiple enzymes involved in lipid metabolism, facilitates the efficient channeling of fatty acids from TGs into phospholipids unless cells experience extensive lipid overload, with potential implications for disease prevention. The liver and body weight of the treated mice were reduced accordingly. We conclude that silybin buffers excessive hepatic TG accumulation, a hallmark of MAFLD, and redirects fatty acids by limiting phospholipid degradation and stimulating (energy-consuming) phospholipid biosynthesis and possibly membrane biogenesis.

Gavage of silymarin/silybin to mice reduced pathological changes in liver and serum lipid composition [54,62,63,183,184], and its beneficial effects were anticipated to depend on either a decreased cholesterol/phospholipid ratio [62], a reduced proportion of SM relative to PC [62,183], or increased PE levels [63]. Our lipidomic analysis essentially confirmed an efficient upregulation of PE and other glycerophospholipids (rather than sphingolipids) in mouse liver by silybin. The influence on membrane properties is difficult to assess, but the homogeneous upregulation of phospholipid classes suggests that there are no major changes. It should be noted that we did not analyze free cholesterol, a major membrane component that affects rigidity and fluidity [185].

Structural aspects of silybin A for the induction of a metabolic switch

Structure-activity relationship studies underscore that silybin functionally intervenes at two (or more) different sites in lipid metabolism to accomplish the shift from TGs to phospholipids. While the saturation of the flavonoid scaffold at the 2,3-position is essential for phospholipid accumulation (but has little effect on the amount of cellular TG), changes in

the stereochemistry at the dioxan ring reduced both the effect on phospholipid and TG levels. The introduction of a 2,3-double bond yielding 2,3-dehydrosilybin even resulted in a decrease of the PS and PG content. The biosynthesis of these acidic phospholipids requires the conversion of DAG to phosphatidic acid, whereas PC and PE can be synthesized directly from DAG (Figure 7) [186]. Interestingly, the ring rearrangement in the hemiacetal did not substantially hamper the activity on phospholipids or TGs when compared to the diastereomeric silybin mixture. Together, silybin modulates phospholipid and TG metabolism through independent pathways, with the magnitude and directionality of the effect strongly dependent on the stereochemistry and saturation of the flavonolignan. Consistent with the hypothesis that silybin upregulates the intracellular phospholipid content also independently of the decrease in TGs, pharmacological inhibition of specific isoenzymes involved in lipid droplet degradation (ATGL) or lipid droplet biogenesis (DGAT2) did not markedly alter the cellular phospholipid content.

Impact of silymarin/silybin on drug-metabolizing enzymes

We also show that silymarin/silybin increases the content of phospholipids in hepatocytes, thereby forming intracellular membranes that are likely to host enzymes involved in biotransformation. On the one hand, phase I and phase II enzymes provide protection against multiple xenobiotics and diminish drug-induced hepatotoxicity [187]. On the other hand, phase I CYP enzymes convert various xenobiotics, e.g., the analgesic drug acetaminophen (paracetamol), into toxic metabolites [188]. Silymarin has been proposed to protect against toxic liver injury i) by inhibiting CYP enzymes and suppressing deleterious metabolism, ii) by inducing the expression of phase II enzymes such as UGT and GST, and iii) by upregulating membrane transporters that enhance the excretion of xenobiotics [137,138]. While our data confirm an upregulation of phase II enzyme activities by silybin, we found that not only the

expression but also the activity of multiple CYP isoenzymes was increased rather than decreased under short-term treatment. We suggest that the mixed outcomes of studies investigating the effect of silymarin/silybin on CYP enzymes originate from kinetic regulation and the competition between CYP expression and inhibition, which seems to be sensitive to the dosage, route of application, formulation, and/or duration of treatment [101,137,139]. Thus, the elevated CYP enzyme activity in our experimental design is likely due to an increased CYP protein expression that masks the inhibitory effect of silybin on CYP activity. In support of this hypothesis, silymarin administration to rats increased the hepatic cytochrome P450 levels with defined kinetics [189], as further validated here at the transcriptome level in HCV-infected mice treated with silybin. Overall, silymarin/silybin induced a rapid upregulation of drug-metabolizing enzymes, followed by a decrease in expression with prolonged treatment. Another factor that may contribute to the variable study results on CYP enzymes is that healthy and diseased tissues seem to respond differently to silybin. In fact, silymarin/silybin partially restores CYP enzyme homeostasis under pathophysiological conditions [141,142,144], whereas effects in healthy individuals are more diverse [140,145,152]. It should be noted that, with a few exceptions, most *in vivo* animal and human studies have failed to confirm that silymarin/silybin substantially interferes with the pharmacokinetics of various drugs that are metabolized by CYP enzymes [36]. However, one of the few studies showing significant effects in healthy volunteers found, consistent with our results in mice, that silymarin (140 mg, daily) increased the clearance and decreased the C_{max} values of metronidazole, a drug that is metabolized by CYP3A4 and CYP2C9 [190]. Whether the modulation of CYP enzyme activity by silymarin is of clinical relevance in patients with MAFLD remains elusive and needs to be systematically evaluated for specific formulations, dosages and CYP isoenzymes in future kinetic studies.

Efficacy of silymarin/silybin in the treatment of MAFLD

Given the mixed results of silymarin/silybin on lipid metabolism in health and disease [131-136], we investigated the ability of silybin to redirect lipid metabolism in *in vitro* models of MAFLD (achieved by massive fatty acid overload) and acute lipotoxicity (induced by excess saturated fatty acids). On the one hand, silybin A consistently reduced lipid droplet content below basal levels in unstressed and fatty acid-challenged hepatocytes, notably superior to selective inhibitors of DGAT1 or DGAT2 or antagonist of PPARγ. On the other hand, silybin A was considerably less effective in redirecting fatty acids from lipid droplets to phospholipids in stressed as compared to non-stressed cells and did not protect against lipotoxicity. Our results suggest that the silymarin/silybin-induced lipid class switch from TGs to phospholipids is particularly effective in protecting against adverse dysregulation of lipid metabolism in normal and pre-disease conditions, whereas the beneficial effects appear to be largely limited to reducing TGs in liver diseases associated with severe TG accumulation, such as MAFLD. Further studies are needed to elucidate the general relevance of this dual mechanism by directly comparing healthy and diseased states in clinical trials.

Differences between the effects of silymarin and silybin

Silymarin and silybin modulate lipid metabolism in hepatocytes in a comparable manner, but there are also substantial differences, and some effects are seen only for silymarin or silybin.

First, only silymarin elevated the levels of butyryl-CoA, an intermediate of β-oxidation (1.5-fold), implying that fatty acid degradation is stimulated by components of silymarin other than silybin. Whether such polypharmacological modulation by silymarin has advantages, is poorly understood. On the one hand, we discussed above that excessive β-oxidation under stress conditions could be detrimental due to the production of reactive oxygen species

(ROS)[14]. On the other hand, the induction of fatty acid catabolism by silymarin is moderate and could help to meet the energy demands for stress-adaptive, regenerative pathways (including lipid remodeling), especially since the antioxidants in silymarin already counteract ROS accumulation [191].

Second, we observed significant differences in the effect of silymarin and silybin on triglyceride levels in different cell types. Whereas silybin significantly reduces TG levels in hepatocytes and has no effect in monocytes, silymarin hardly affects TG levels in hepatocytes but robustly decreases them in monocytes. While the accumulation of TGs in hepatocytes is critical for the development of MAFLD, the extent to which reducing TGs in monocytes benefits the disease process is not well understood.

Third, silymarin and silybin clearly differ in how they manipulate the expression of lipid-metabolizing enzymes, although some of the effects may be related to the use of different model systems, which is a limitation of this study. For example, the expression of DGAT2 is significantly downregulated only in hepatocytes isolated from silybin-treated mice, without effects in silymarin-treated HepG2 and Huh7.5.1 liver cells. However, reduced expression of DGAT1 is observed in both hepatocytes from silybin-treated mice and silymarin-treated HepG2 and Huh7.5.1 cells, suggesting that the repression of DGAT2 is silybin-specific. Additional differential effects are seen in the regulation of phospholipases: PLA2G1B is downregulated in hepatocytes from silybin-treated mice, whereas PLD1 is downregulated in silymarin-treated HepG2 and Huh7.5.1 cells.

In addition to modulating lipid metabolism, silymarin is known to have beneficially effects on other pathogenic mechanisms associated with MAFLD, such as inflammation and glucose metabolism [192], the latter of which is also supported by our data.

Conclusion

The milk thistle extract silymarin and its bioactive component silybin have unique lipid-modulating properties. Rather than targeting one particular pathway, silymarin/silybin affects lipid metabolism at multiple hubs. In hepatic pre-disease states, silybin decreases TG content, while attenuating phospholipid degradation and stimulating phospholipid biosynthesis. In combination with the parallel reprogramming of phase I and II metabolism, this lipid class switch seems to expand functional intracellular membranes and redirects the hepatic biotransformation capacity. Considering that the selective inhibition of TG biosynthesis actually enhances liver damage, as suggested by preclinical studies with DGAT2 antisense oligonucleotide treatment [6], we propose that the lipid metabolic switch from TGs to phospholipids in hepatocytes and potentially other liver cells (i.e., Kupffer cells) and extrahepatic cells critically contributes to the liver-protective (rather than disease-alleviating) function of silybin. The beneficial reprogramming of lipid metabolism is based on the absolute configuration of silybin as well as the saturation of ring C in the flavonoid scaffold at the 2,3-position. These structural aspects contribute differentially to the TG-lowering and phospholipid-accumulating activities of silybin, and structural modifications realized in minor components of milk thistle allow dissection of both activities.

In conclusion, our results shed light on the mechanisms underlying liver protection by silymarin/silybin under physiological and pathophysiological conditions. Although silymarin/silybin appears to have the potential to improve the biochemical hallmarks of MAFLD and may be beneficial in mild forms of the disease through the mechanisms proposed here, our data suggest that this mechanism may be less effective or even ineffective in severe disease states. Whether silymarin/silybin exerts beneficial effects under these conditions when combined with adjunctive supplements or dietary restriction remains elusive. Future evidence-based studies with a larger number of participants and longer follow-up are

needed to explore the relevance of the silybin A-induced lipid metabolic switch in humans, both for disease prevention and under pathophysiological conditions.

Abbreviations ACC, acetyl-CoA carboxylase; ACOX3, acyl-CoA oxidase 3, pristanoyl; ACOT7, acyl-CoA thioesterase 7; ACSL6, acyl-CoA synthetase long chain family member 6; ATF6, activating transcription factor; ATGL, adipocyte triglyceride lipase; BSA, bovine serum albumin; CE, cholesteryl esters; CL, chemiluminescence; CPT1a, carnitine palmitoyl-transferase 1α; CYP, cytochrome P_{450}; DAG, diacylglycerol; DGAT, diacylglycerol-O-acyltransferase; ER, endoplasmic reticulum; FASN, fatty acid synthase; GPAM, glycerol-3-phosphate acyltransferase, mitochondrial; GPAT, glycerophosphate acyltransferase; GPX, glutathione peroxidase; GSH, glutathione; GSSG, glutathione disulfide; GST, glutathione S-transferase; HAO2, hydroxyacid oxidase 2; HCV, hepatitis C virus; HSD17B13, 17-beta-hydroxysteroid dehydrogenase 13; LPIAT1, lysophosphatidylinositol acyltransferase 1; LPIN2, Lipin 2; LPAAT, lysophosphatidic acid acyltransferase; LPLAT, lysophospholipid acyltransferase; MBOAT7, membrane-bound O-acyltransferase domain-containing 7; MAFLD, metabolic dysfunction-associated steatotic liver disease; MASH, metabolic dysfunction-associated steatohepatitis; NAFLD, non-alcoholic fatty liver disease; NASH, non-alcoholic steatohepatitis; PC, phosphatidylcholine; PE, phosphatidylethanolamine; PG, phosphatidylglycerol; PI, phosphatidylinositol; PNPLA, patatin-like phospholipase domain-containing; PLA1A, phospholipases A1; PLA2, phospholipase A2; iPLA2/PLA2G6, calcium-independent phospholipase A2 / phospholipase A2 Group VI; PLA2G7, phospholipase A2 Group VII; PLD1, phospholipase D1; PRDX6, peroxiredoxin 6; PS, phosphatidylserine; ROS, reactive oxygen species; SCD5, stearoyl-CoA desaturase 5; SM, sphingomyelin; SREBF, sterol regulatory element binding transcription factor 1; TG, triglyceride; UGT; UDP-glucuronosyltransferase; UPR, unfolded protein response; XBP1s, spliced form of X-box-binding protein 1.

Acknowledgment

Funding: Research activities of the authors related to the subject of this article were supported by the Global Research Initiative 2013/2014 (Bionorica SE), the Deutsche Forschungsgemeinschaft (DFG, German Research Foundation) [KO 4589/4-1], Bionorica Research GmbH (#320092), and the Phospholipid Research Center Heidelberg (AKO-2019-070/2-1 and AKO-2015-037/1-1). Moreover, we acknowledge AIPRAS Onlus (Associazione Italiana per la Promozione delle Ricerche sull'Ambiente e la Saluta umana) for grants in support of this investigation. The authors acknowledge the financial support by the University of Graz. Illustrations were created with BioRender.com

The above-mentioned funding sources were neither involved in study design, data collection, analysis, and interpretation nor in writing and submission of the manuscript.

Author contributions

Solveigh Koeberle: Conceptualization, Data Curation, Formal analysis, Supervision, Visualization, Writing - Original Draft, Writing - Review & Editing. Maria Thürmer: Investigation, Methodology, Visualization, Writing - Review & Editing. Fengting Su: Investigation, Methodology, Visualization, Review & Editing. Markus Werner: Investigation, Writing - Review & Editing. Julia Grander: Investigation, Visualization. Laura Hofer: Investigation. André Gollowitzer: Investigation, Writing - Review & Editing. Loc Le Xuan: Investigation. Felix Benscheidt: Investigation. Ehsan Bonyadirad: Investigation. Armando Zarrelli: Methodology, Writing - Review & Editing. Giovanni Di Fabio: Methodology, Writing - Review & Editing. Oliver Werz: Writing - Review & Editing. Valeria Romanucci: Funding acquisition, Investigation, Methodology, Writing - Review & Editing. Amelie Lupp: Investigation, Methodology, Writing - Review & Editing. Andreas Koeberle:

Conceptualization, Data Curation, Formal analysis, Funding acquisition, Project administration, Supervision, Visualization, Writing - Original Draft, Writing - Review & Editing.

Competing interests

AK received grant support from and was an advisor to Bionorica SE. AK and OW performed contract research for Bionorica SE. The other authors declare no conflicts of interest.

Declaration of Generative AI and AI-assisted technologies in the writing process

During the preparation of this work the authors used ChatGPT3.5 and DeepLWrite in order to improve readability and language. After using these tools, the authors reviewed and edited the content as needed and take full responsibility for the content of the publication.

References

1. Rinella ME, Lazarus JV, Ratziu V, Francque SM, Sanyal AJ, Kanwal F, et al. A multisociety delphi consensus statement on new fatty liver disease nomenclature. Hepatology. 2023; 78: 1966-86.
2. Loomba R, Friedman SL, Shulman GI. Mechanisms and disease consequences of nonalcoholic fatty liver disease. Cell. 2021; 184: 2537-64.
3. Meex RCR, Watt MJ. Hepatokines: Linking nonalcoholic fatty liver disease and insulin resistance. Nat Rev Endocrinol. 2017; 13: 509-20.
4. Perry RJ, Samuel VT, Petersen KF, Shulman GI. The role of hepatic lipids in hepatic insulin resistance and type 2 diabetes. Nature. 2014; 510: 84-91.
5. Younossi ZM, Koenig AB, Abdelatif D, Fazel Y, Henry L, Wymer M. Global epidemiology of nonalcoholic fatty liver disease-meta-analytic assessment of prevalence, incidence, and outcomes. Hepatology. 2016; 64: 73-84.
6. Yamaguchi K, Yang L, Mccall S, Huang J, Yu XX, Pandey SK, et al. Inhibiting triglyceride synthesis improves hepatic steatosis but exacerbates liver damage and fibrosis in obese mice with nonalcoholic steatohepatitis. Hepatology. 2007; 45: 1366-74.
7. Baldini F, Bartolozzi A, Ardito M, Voci A, Portincasa P, Vassalli M, et al. Biomechanics of cultured hepatic cells during different steatogenic hits. J Mech Behav Biomed Mater. 2019; 97: 296-305.
8. Feng B, Meng R, Huang B, Shen S, Bi Y, Zhu D. Silymarin alleviates hepatic oxidative stress and protects against metabolic disorders in high-fat diet-fed mice. Free Radic Res. 2016; 50: 314-27.
9. Hellerbrand C, Schattenberg JM, Peterburs P, Lechner A, Brignoli R. The potential of silymarin for the treatment of hepatic disorders. Clin Phytosci. 2017; 2.
10. Seebacher F, Zeigerer A, Kory N, Krahmer N. Hepatic lipid droplet homeostasis and fatty liver disease. Semin Cell Dev Biol. 2020; 108: 72-81.
11. Danielli M, Perne L, Jarc Jovicic E, Petan T. Lipid droplets and polyunsaturated fatty acid trafficking: Balancing life and death. Front Cell Dev Biol. 2023; 11: 1104725.
12. Jarc E, Petan T. Lipid droplets and the management of cellular stress. Yale J Biol Med. 2019; 92: 435-52.
13. Olzmann JA, Carvalho P. Dynamics and functions of lipid droplets. Nat Rev Mol Cell Biol. 2019; 20: 137-55.
14. Baldini F, Portincasa P, Grasselli E, Damonte G, Salis A, Bonomo M, et al. Aquaporin-9 is involved in the lipid-lowering activity of the nutraceutical silybin on hepatocytes through modulation of autophagy and lipid droplets composition. Biochim Biophys Acta Mol Cell Biol Lipids. 2020; 1865: 158586.
15. Su F, Koeberle A. Regulation and targeting of srebp-1 in hepatocellular carcinoma. Cancer Metastasis Rev. 2023.
16. Wang CW. Lipid droplets, lipophagy, and beyond. Biochim Biophys Acta. 2016; 1861: 793-805.
17. Vergani L. Fatty acids and effects on in vitro and in vivo models of liver steatosis. Curr Med Chem. 2019; 26: 3439-56.
18. Malhi H, Gores GJ. Molecular mechanisms of lipotoxicity in nonalcoholic fatty liver disease. Semin Liver Dis. 2008; 28: 360-9.
19. Eslam M, Valenti L, Romeo S. Genetics and epigenetics of nafld and nash: Clinical impact. J Hepatol. 2018; 68: 268-79.
20. Sookoian S, Pirola CJ, Valenti L, Davidson NO. Genetic pathways in nonalcoholic fatty liver disease: Insights from systems biology. Hepatology. 2020; 72: 330-46.

21. Chen F, Zhou Y, Wu Z, Li Y, Zhou W, Wang Y. Integrated analysis of key genes and pathways involved in nonalcoholic steatohepatitis improvement after roux-en-y gastric bypass surgery. Front Endocrinol (Lausanne). 2020; 11: 611213.
22. Fuchs CD, Radun R, Dixon ED, Mlitz V, Timelthaler G, Halilbasic E, et al. Hepatocyte-specific deletion of adipose triglyceride lipase (adipose triglyceride lipase/patatin-like phospholipase domain containing 2) ameliorates dietary induced steatohepatitis in mice. Hepatology. 2022; 75: 125-39.
23. Teslovich TM, Musunuru K, Smith AV, Edmondson AC, Stylianou IM, Koseki M, et al. Biological, clinical and population relevance of 95 loci for blood lipids. Nature. 2010; 466: 707-13.
24. Chamulitrat W, Jansakun C, Li H, Liebisch G. Rescue of hepatic phospholipid remodeling defectin ipla2beta-null mice attenuates obese but not non-obese fatty liver. Biomolecules. 2020; 10, 1332.
25. Kienesberger PC, Oberer M, Lass A, Zechner R. Mammalian patatin domain containing proteins: A family with diverse lipolytic activities involved in multiple biological functions. J Lipid Res. 2009; 50 Suppl: S63-8.
26. Kim KY, Jang HJ, Yang YR, Park KI, Seo J, Shin IW, et al. Srebp-2/pnpla8 axis improves non-alcoholic fatty liver disease through activation of autophagy. Sci Rep. 2016; 6: 35732.
27. Shen W, Yang L, Yang Y, Wang P, Tao X, Shen Y, et al. Prdx6 promotes fatty acid oxidation via pla2-dependent pparalpha activation in rats fed high-fat diet. Antioxid Redox Signal. 2023; 38: 1184-200.
28. Wang H, Zhao Y, Pan Y, Yang A, Li C, Wang S, et al. Inhibition of phospholipase d1 ameliorates hepatocyte steatosis and non-alcoholic fatty liver disease. JHEP Rep. 2023; 5: 100726.
29. Tanaka Y, Shimanaka Y, Caddeo A, Kubo T, Mao Y, Kubota T, et al. Lpiat1/mboat7 depletion increases triglyceride synthesis fueled by high phosphatidylinositol turnover. Gut. 2021; 70: 180-93.
30. Trepo E, Valenti L. Update on nafld genetics: From new variants to the clinic. J Hepatol. 2020; 72: 1196-209.
31. Abul-Husn NS, Cheng X, Li AH, Xin Y, Schurmann C, Stevis P, et al. A protein-truncating hsd17b13 variant and protection from chronic liver disease. N Engl J Med. 2018; 378: 1096-106.
32. Paul B, Lewinska M, Andersen JB. Lipid alterations in chronic liver disease and liver cancer. JHEP Rep. 2022; 4: 100479.
33. Ooi GJ, Meikle PJ, Huynh K, Earnest A, Roberts SK, Kemp W, et al. Hepatic lipidomic remodeling in severe obesity manifests with steatosis and does not evolve with non-alcoholic steatohepatitis. J Hepatol. 2021; 75: 524-35.
34. Mannisto V, Kaminska D, Karja V, Tiainen M, De Mello VD, Hanhineva K, et al. Total liver phosphatidylcholine content associates with non-alcoholic steatohepatitis and glycine n-methyltransferase expression. Liver Int. 2019; 39: 1895-905.
35. Puri P, Baillie RA, Wiest MM, Mirshahi F, Choudhury J, Cheung O, et al. A lipidomic analysis of nonalcoholic fatty liver disease. Hepatology. 2007; 46: 1081-90.
36. Tvrdy V, Pourova J, Jirkovsky E, Kren V, Valentova K, Mladenka P. Systematic review of pharmacokinetics and potential pharmacokinetic interactions of flavonolignans from silymarin. Med Res Rev. 2021; 41: 2195-246.
37. Rainone F. Milk thistle. Am Fam Physician. 2005; 72: 1285-8.
38. Abenavoli L, Capasso R, Milic N, Capasso F. Milk thistle in liver diseases: Past, present, future. Phytother Res. 2010; 24: 1423-32.

39. Yan T, Yan N, Wang P, Xia Y, Hao H, Wang G, et al. Herbal drug discovery for the treatment of nonalcoholic fatty liver disease. Acta Pharm Sin B. 2020; 10: 3-18.
40. Stolf AM, Cardoso CC, Acco A. Effects of silymarin on diabetes mellitus complications: A review. Phytother Res. 2017; 31: 366-74.
41. Kren V. Chirality matters: Biological activity of optically pure silybin and its congeners. Int J Mol Sci. 2021; 22: 7885.
42. Milic N, Milosevic N, Suvajdzic L, Zarkov M, Abenavoli L. New therapeutic potentials of milk thistle (silybum marianum). Nat Prod Commun. 2013; 8: 1801-10.
43. Biedermann D, Vavrikova E, Cvak L, Kren V. Chemistry of silybin. Nat Prod Rep. 2014; 31: 1138-57.
44. Fenclova M, Stranska-Zachariasova M, Benes F, Novakova A, Jonatova P, Kren V, et al. Liquid chromatography-drift tube ion mobility-mass spectrometry as a new challenging tool for the separation and characterization of silymarin flavonolignans. Anal Bioanal Chem. 2020; 412: 819-32.
45. Bagherniya M, Nobili V, Blesso CN, Sahebkar A. Medicinal plants and bioactive natural compounds in the treatment of non-alcoholic fatty liver disease: A clinical review. Pharmacol Res. 2018; 130: 213-40.
46. Wang L, Yan Y, Wu L, Peng J. Natural products in non-alcoholic fatty liver disease (nafld): Novel lead discovery for drug development. Pharmacol Res. 2023; 196: 106925.
47. Federico A, Dallio M, Loguercio C. Silymarin/silybin and chronic liver disease: A marriage of many years. Molecules. 2017; 22: 191.
48. Kalopitas G, Antza C, Doundoulakis I, Siargkas A, Kouroumalis E, Germanidis G, et al. Impact of silymarin in individuals with nonalcoholic fatty liver disease: A systematic review and meta-analysis. Nutrition. 2021; 83: 111092.
49. Anushiravani A, Haddadi N, Pourfarmanbar M, Mohammadkarimi V. Treatment options for nonalcoholic fatty liver disease: A double-blinded randomized placebo-controlled trial. Eur J Gastroenterol Hepatol. 2019; 31: 613-7.
50. Niu H, Sanabria-Cabrera J, Alvarez-Alvarez I, Robles-Diaz M, Stankeviciute S, Aithal GP, et al. Prevention and management of idiosyncratic drug-induced liver injury: Systematic review and meta-analysis of randomised clinical trials. Pharmacol Res. 2021; 164: 105404.
51. Saller R, Brignoli R, Melzer J, Meier R. An updated systematic review with meta-analysis for the clinical evidence of silymarin. Forsch Komplementmed. 2008; 15: 9-20.
52. Bahmani M, Shirzad H, Rafieian S, Rafieian-Kopaei M. Silybum marianum: Beyond hepatoprotection. J Evid Based Complementary Altern Med. 2015; 20: 292-301.
53. Fraschini F, Demartini, G. & Esposti, D. Pharmacology of silymarin. Clin. Drug Investig. 2002; 22: 51–65.
54. Stiuso P, Scognamiglio I, Murolo M, Ferranti P, De Simone C, Rizzo MR, et al. Serum oxidative stress markers and lipidomic profile to detect nash patients responsive to an antioxidant treatment: A pilot study. Oxid Med Cell Longev. 2014; 2014: 169216.
55. Ni X, Wang H. Silymarin attenuated hepatic steatosis through regulation of lipid metabolism and oxidative stress in a mouse model of nonalcoholic fatty liver disease (nafld). Am J Transl Res. 2016; 8: 1073-81.
56. Huseini HF, Larijani B, Heshmat R, Fakhrzadeh H, Radjabipour B, Toliat T, et al. The efficacy of silybum marianum (l.) gaertn. (silymarin) in the treatment of type ii diabetes: A randomized, double-blind, placebo-controlled, clinical trial. Phytother Res. 2006; 20: 1036-9.

57. Sobolova L, Skottova N, Vecera R, Urbanek K. Effect of silymarin and its polyphenolic fraction on cholesterol absorption in rats. Pharmacol Res. 2006; 53: 104-12.
58. Nassuato G, Iemmolo RM, Strazzabosco M, Lirussi F, Deana R, Francesconi MA, et al. Effect of silibinin on biliary lipid composition. Experimental and clinical study. J Hepatol. 1991; 12: 290-5.
59. Voroneanu L, Nistor I, Dumea R, Apetrii M, Covic A. Silymarin in type 2 diabetes mellitus: A systematic review and meta-analysis of randomized controlled trials. J Diabetes Res. 2016; 2016: 5147468.
60. Sun WL, Hua S, Li XY, Shen L, Wu H, Ji HF. Microbially produced vitamin b12 contributes to the lipid-lowering effect of silymarin. Nat Commun. 2023; 14: 477.
61. Schriewer H, Weinhold F. The influence of silybin from silybum marianum (l.) gaertn. On in vitro phosphatidyl choline biosynthesis in rat livers. Arzneimittelforschung. 1979; 29: 791-2.
62. Muriel P, Mourelle M. Prevention by silymarin of membrane alterations in acute ccl4 liver damage. J Appl Toxicol. 1990; 10: 275-9.
63. Schriewer H, Lohmann J, Rauen HM. [the effect of silybin-dihemisuccinate on regulation disorders in phospholipid metabolism in acute galactosamine intoxication in the rat]. Arzneimittelforschung. 1975; 25: 1582-5.
64. Hermansson M, Hokynar K, Somerharju P. Mechanisms of glycerophospholipid homeostasis in mammalian cells. Prog Lipid Res. 2011; 50: 240-57.
65. Di Fabio G, Romanucci V, Di Marino C, De Napoli L, Zarrelli A. A rapid and simple chromatographic separation of diastereomers of silibinin and their oxidation to produce 2,3-dehydrosilybin enantiomers in an optically pure form. Planta Med. 2013; 79: 1077-80.
66. Di Fabio GR, V.; De Nisco, M.; Pedatella, S.; Di Marino, C.; Zarrelli, A. Microwave-assisted oxidation of silibinin: A simple and preparative method for the synthesis of improved radical scavengers. Tetrahedron Lett. 2013; 54: 6279–82.
67. Pein H, Ville A, Pace S, Temml V, Garscha U, Raasch M, et al. Endogenous metabolites of vitamin e limit inflammation by targeting 5-lipoxygenase. Nat Commun. 2018; 9: 3834.
68. Koeberle A, Munoz E, Appendino GB, Minassi A, Pace S, Rossi A, et al. Sar studies on curcumin's pro-inflammatory targets: Discovery of prenylated pyrazolocurcuminoids as potent and selective novel inhibitors of 5-lipoxygenase. J Med Chem. 2014; 57: 5638-48.
69. Koeberle A, Shindou H, Harayama T, Shimizu T. Role of lysophosphatidic acid acyltransferase 3 for the supply of highly polyunsaturated fatty acids in tm4 sertoli cells. FASEB J. 2010; 24: 4929-38.
70. Koeberle A, Shindou H, Harayama T, Yuki K, Shimizu T. Polyunsaturated fatty acids are incorporated into maturating male mouse germ cells by lysophosphatidic acid acyltransferase 3. FASEB J. 2012; 26: 169-80.
71. Espada L, Dakhovnik A, Chaudhari P, Martirosyan A, Miek L, Poliezhaieva T, et al. Loss of metabolic plasticity underlies metformin toxicity in aged caenorhabditis elegans. Nat Metab. 2020; 2: 1316-31.
72. Koeberle A, Shindou H, Koeberle SC, Laufer SA, Shimizu T, Werz O. Arachidonoyl-phosphatidylcholine oscillates during the cell cycle and counteracts proliferation by suppressing akt membrane binding. Proc Natl Acad Sci U S A. 2013; 110: 2546-51.
73. Koeberle A, Pergola C, Shindou H, Koeberle SC, Shimizu T, Laufer SA, et al. Role of p38 mitogen-activated protein kinase in linking stearoyl-coa desaturase-1 activity with endoplasmic reticulum homeostasis. FASEB J. 2015; 29: 2439-49.

74. Thürmer M, Gollowitzer A, Pein H, Neukirch K, Gelmez E, Waltl L, et al. Pi(18:1/18:1) is a scd1-derived lipokine that limits stress signaling. Nat Commun. 2022; 13: 2982.
75. Liao S, Gollowitzer A, Bormel L, Maier C, Gottschalk L, Werz O, et al. Alpha-tocopherol-13'-carboxychromanol induces cell cycle arrest and cell death by inhibiting the srebp1-scd1 axis and causing imbalance in lipid desaturation. Int J Mol Sci. 2023; 24: 9229.
76. Van Pijkeren A, Egger AS, Hotze M, Zimmermann E, Kipura T, Grander J, et al. Proteome coverage after simultaneous proteo-metabolome liquid-liquid extraction. J Proteome Res. 2023; 22: 951-66.
77. Schwab A, Rao Z, Zhang J, Gollowitzer A, Siebenkas K, Bindel N, et al. Zeb1 mediates emt/plasticity-associated ferroptosis sensitivity in cancer cells by regulating lipogenic enzyme expression and phospholipid composition. Nat Cell Biol. 2024; 26: 1470–81.
78. Glatzel DK, Koeberle A, Pein H, Loser K, Stark A, Keksel N, et al. Acetyl-coa carboxylase 1 regulates endothelial cell migration by shifting the phospholipid composition. J Lipid Res. 2018; 59: 298-311.
79. Ewels P, Magnusson M, Lundin S, Kaller M. Multiqc: Summarize analysis results for multiple tools and samples in a single report. Bioinformatics. 2016; 32: 3047-8.
80. Dobin A, Davis CA, Schlesinger F, Drenkow J, Zaleski C, Jha S, et al. Star: Ultrafast universal rna-seq aligner. Bioinformatics. 2013; 29: 15-21.
81. Anders S, Pyl PT, Huber W. Htseq--a python framework to work with high-throughput sequencing data. Bioinformatics. 2015; 31: 166-9.
82. Love MI, Huber W, Anders S. Moderated estimation of fold change and dispersion for rna-seq data with deseq2. Genome Biol. 2014; 15: 550.
83. Hsiang CY, Lin LJ, Kao ST, Lo HY, Chou ST, Ho TY. Glycyrrhizin, silymarin, and ursodeoxycholic acid regulate a common hepatoprotective pathway in hepg2 cells. Phytomedicine. 2015; 22: 768-77.
84. Lovelace ES, Wagoner J, Macdonald J, Bammler T, Bruckner J, Brownell J, et al. Silymarin suppresses cellular inflammation by inducing reparative stress signaling. J Nat Prod. 2015; 78: 1990-2000.
85 Debroy S, Hiraga N, Imamura M, Hayes CN, Akamatsu S, Canini L, et al. Hepatitis c virus dynamics and cellular gene expression in upa-scid chimeric mice with humanized livers during intravenous silibinin monotherapy. J Viral Hepat. 2016; 23: 708-17.
86. Barrett T, Wilhite SE, Ledoux P, Evangelista C, Kim IF, Tomashevsky M, et al. Ncbi geo: Archive for functional genomics data sets--update. Nucleic Acids Res. 2013; 41: D991-5.
87. Lupp A, Nagel F, Schulz S. Reevaluation of sst(1) somatostatin receptor expression in human normal and neoplastic tissues using the novel rabbit monoclonal antibody umb-7. Regul Pept. 2013; 183: 1-6.
88. Ellman GL. Tissue sulfhydryl groups. Arch Biochem Biophys. 1959; 82: 70-7.
89. Hissin PJ, Hilf R. A fluorometric method for determination of oxidized and reduced glutathione in tissues. Anal Biochem. 1976; 74: 214-26.
90. Yagi T, Day RS, 3rd. Differential sensitivities of transformed and untransformed murine cell lines to DNA cross-linking agents relative to repair of o6-methylguanine. Mutat Res. 1987; 184: 223-7.
91. Klinger W, Muller D. The influence of age on the protein concentration in serum, liver and kidney of rats determined by various methods. Z Versuchstierkd. 1974; 16: 149-53.
92. Lubet RA, Mayer RT, Cameron JW, Nims RW, Burke MD, Wolff T, et al. Dealkylation of pentoxyresorufin: A rapid and sensitive assay for measuring induction of cytochrome(s) p-450 by phenobarbital and other xenobiotics in the rat. Arch Biochem Biophys. 1985; 238: 43-8.

93. Aitio A. A simple and sensitive assay of 7-ethoxycoumarin deethylation. Anal Biochem. 1978; 85: 488-91.
94. Pohl RJ, Fouts JR. A rapid method for assaying the metabolism of 7-ethoxyresorufin by microsomal subcellular fractions. Anal Biochem. 1980; 107: 150-5.
95. Kleeberg U, Klinger W. Sensitive formaldehyde determination with nash's reagent and a 'tryptophan reaction'. J Pharmacol Methods. 1982; 8: 19-31.
96. Habig WH, Pabst MJ, Jakoby WB. Glutathione s-transferases. The first enzymatic step in mercapturic acid formation. J Biol Chem. 1974; 249: 7130-9.
97. Lilienblum W, Walli AK, Bock KW. Differential induction of rat liver microsomal udp-glucuronosyltransferase activites by various inducing agents. Biochem Pharmacol. 1982; 31: 907-13.
98. Bock KW, Burchell B, Dutton GJ, Hanninen O, Mulder GJ, Owens IS, et al. Udp-glucuronosyltransferase activities. Guidelines for consistent interim terminology and assay conditions. Biochem Pharmacol. 1983; 32: 953-5.
99. Bhatt-Wessel B, Jordan TW, Miller JH, Peng L. Role of dgat enzymes in triacylglycerol metabolism. Arch Biochem Biophys. 2018; 655: 1-11.
100. Christodoulou E, Kechagia IA, Tzimas S, Balafas E, Kostomitsopoulos N, Archontaki H, et al. Serum and tissue pharmacokinetics of silibinin after per os and i.V. Administration to mice as a hp-beta-cd lyophilized product. Int J Pharm. 2015; 493: 366-73.
101. Zhao J, Agarwal R. Tissue distribution of silibinin, the major active constituent of silymarin, in mice and its association with enhancement of phase ii enzymes: Implications in cancer chemoprevention. Carcinogenesis. 1999; 20: 2101-8.
102. Perona JS. Membrane lipid alterations in the metabolic syndrome and the role of dietary oils. Biochim Biophys Acta Biomembr. 2017; 1859: 1690-703.
103. Van Meer G, Voelker DR, Feigenson GW. Membrane lipids: Where they are and how they behave. Nat Rev Mol Cell Biol. 2008; 9: 112-24.
104. Liu Y, Xu W, Zhai T, You J, Chen Y. Silibinin ameliorates hepatic lipid accumulation and oxidative stress in mice with non-alcoholic steatohepatitis by regulating cflar-jnk pathway. Acta Pharm Sin B. 2019; 9: 745-57.
105. Vecchione G, Grasselli E, Cioffi F, Baldini F, Oliveira PJ, Sardao VA, et al. The nutraceutic silybin counteracts excess lipid accumulation and ongoing oxidative stress in an in vitro model of non-alcoholic fatty liver disease progression. Front Nutr. 2017; 4: 42.
106. Feng R, Chen JH, Liu CH, Xia FB, Xiao Z, Zhang X, et al. A combination of pueraria lobata and silybum marianum protects against alcoholic liver disease in mice. Phytomedicine. 2019; 58: 152824.
107. Sun R, Xu D, Wei Q, Zhang B, Aa J, Wang G, et al. Silybin ameliorates hepatic lipid accumulation and modulates global metabolism in an nafld mouse model. Biomed Pharmacother. 2020; 123: 109721.
108. Yang L, Liu Q, Zhang H, Wang Y, Li Y, Chen S, et al. Silibinin improves nonalcoholic fatty liver by regulating the expression of mir122: An in vitro and in vivo study. Mol Med Rep. 2021; 23: 335.
109. Milacic M, Beavers D, Conley P, Gong C, Gillespie M, Griss J, et al. The reactome pathway knowledgebase 2024. Nucleic Acids Res. 2024; 52: D672-D8.
110. Badawi AF, Cavalieri EL, Rogan EG. Role of human cytochrome p450 1a1, 1a2, 1b1, and 3a4 in the 2-, 4-, and 16alpha-hydroxylation of 17beta-estradiol. Metabolism. 2001; 50: 1001-3.

111. Kisselev P, Schunck WH, Roots I, Schwarz D. Association of cyp1a1 polymorphisms with differential metabolic activation of 17beta-estradiol and estrone. Cancer Res. 2005; 65: 2972-8.
112. Schwarz D, Kisselev P, Ericksen SS, Szklarz GD, Chernogolov A, Honeck H, et al. Arachidonic and eicosapentaenoic acid metabolism by human cyp1a1: Highly stereoselective formation of 17(r),18(s)-epoxyeicosatetraenoic acid. Biochem Pharmacol. 2004; 67: 1445-57.
113. Fer M, Corcos L, Dreano Y, Plee-Gautier E, Salaun JP, Berthou F, et al. Cytochromes p450 from family 4 are the main omega hydroxylating enzymes in humans: Cyp4f3b is the prominent player in pufa metabolism. J Lipid Res. 2008; 49: 2379-89.
114. Lucas D, Goulitquer S, Marienhagen J, Fer M, Dreano Y, Schwaneberg U, et al. Stereoselective epoxidation of the last double bond of polyunsaturated fatty acids by human cytochromes p450. J Lipid Res. 2010; 51: 1125-33.
115. Filali-Mouncef Y, Hunter C, Roccio F, Zagkou S, Dupont N, Primard C, et al. The menage a trois of autophagy, lipid droplets and liver disease. Autophagy. 2022; 18: 50-72.
116. Gluchowski NL, Becuwe M, Walther TC, Farese RV, Jr. Lipid droplets and liver disease: From basic biology to clinical implications. Nat Rev Gastroenterol Hepatol. 2017; 14: 343-55.
117. Shi H, Luo J, Zhu J, Li J, Sun Y, Lin X, et al. Ppar gamma regulates genes involved in triacylglycerol synthesis and secretion in mammary gland epithelial cells of dairy goats. PPAR Res. 2013; 2013: 310948.
118. Petan T. Lipid droplets in cancer. Rev Physiol Biochem Pharmacol. 2020.
119. Tang Y, Zhou J, Hooi SC, Jiang YM, Lu GD. Fatty acid activation in carcinogenesis and cancer development: Essential roles of long-chain acyl-coa synthetases. Oncol Lett. 2018; 16: 1390-6.
120. Tong L. Acetyl-coenzyme a carboxylase: Crucial metabolic enzyme and attractive target for drug discovery. Cell Mol Life Sci. 2005; 62: 1784-803.
121. Yamashita A, Hayashi Y, Nemoto-Sasaki Y, Ito M, Oka S, Tanikawa T, et al. Acyltransferases and transacylases that determine the fatty acid composition of glycerolipids and the metabolism of bioactive lipid mediators in mammalian cells and model organisms. Prog Lipid Res. 2014; 53: 18-81.
122. Batchuluun B, Pinkosky SL, Steinberg GR. Lipogenesis inhibitors: Therapeutic opportunities and challenges. Nat Rev Drug Discov. 2022; 21: 283–305.
123. Kleiboeker B, Lodhi IJ. Peroxisomal regulation of energy homeostasis: Effect on obesity and related metabolic disorders. Mol Metab. 2022; 65: 101577.
124. Liang D, Minikes AM, Jiang X. Ferroptosis at the intersection of lipid metabolism and cellular signaling. Mol Cell. 2022; 82: 2215-27.
125. Gan B. Mitochondrial regulation of ferroptosis. J Cell Biol. 2021; 220: e202105043.
126. Araya J, Rodrigo R, Videla LA, Thielemann L, Orellana M, Pettinelli P, et al. Increase in long-chain polyunsaturated fatty acid n - 6/n - 3 ratio in relation to hepatic steatosis in patients with non-alcoholic fatty liver disease. Clin Sci (Lond). 2004; 106: 635-43.
127. Gomez-Lechon MJ, Donato MT, Martinez-Romero A, Jimenez N, Castell JV, O'connor JE. A human hepatocellular in vitro model to investigate steatosis. Chem Biol Interact. 2007; 165: 106-16.
128. Guguen-Guillouzo C, Guillouzo A. General review on in vitro hepatocyte models and their applications. Methods Mol Biol. 2010; 640: 1-40.
129. Da Silva DC, Valentao P, Andrade PB, Pereira DM. Endoplasmic reticulum stress signaling in cancer and neurodegenerative disorders: Tools and strategies to understand its complexity. Pharmacol Res. 2020; 155: 104702.

130. Koeberle A, Loser K, Thurmer M. Stearoyl-coa desaturase-1 and adaptive stress signaling. Biochim Biophys Acta. 2016; 1861: 1719-26.
131. Dallio M, Masarone M, Romeo M, Tuccillo C, Morisco F, Persico M, et al. Pnpla3, tm6sf2, and mboat7 influence on nutraceutical therapy response for non-alcoholic fatty liver disease: A randomized controlled trial. Front Med (Lausanne). 2021; 8: 734847.
132. Federico A, Dallio M, Masarone M, Gravina AG, Di Sarno R, Tuccillo C, et al. Evaluation of the effect derived from silybin with vitamin d and vitamin e administration on clinical, metabolic, endothelial dysfunction, oxidative stress parameters, and serological worsening markers in nonalcoholic fatty liver disease patients. Oxid Med Cell Longev. 2019; 2019: 8742075.
133. Federico A, Dallio M, Gravina AG, Diano N, Errico S, Masarone M, et al. The bisphenol a induced oxidative stress in non-alcoholic fatty liver disease male patients: A clinical strategy to antagonize the progression of the disease. Int J Environ Res Public Health. 2020; 17: 3369.
134. Wah Kheong C, Nik Mustapha NR, Mahadeva S. A randomized trial of silymarin for the treatment of nonalcoholic steatohepatitis. Clin Gastroenterol Hepatol. 2017; 15: 1940-9 e8.
135.. Loguercio C, Andreone P, Brisc C, Brisc MC, Bugianesi E, Chiaramonte M, et al. Silybin combined with phosphatidylcholine and vitamin e in patients with nonalcoholic fatty liver disease: A randomized controlled trial. Free Radic Biol Med. 2012; 52: 1658-65.
136 Lirussi F, Beccarello A, Zanette G, De Monte A, Donadon V, Velussi M, et al. Silybin-beta-cyclodextrin in the treatment of patients with diabetes mellitus and alcoholic liver disease. Efficacy study of a new preparation of an anti-oxidant agent. Diabetes Nutr Metab. 2002; 15: 222-31.
137. Delmas D, Xiao J, Vejux A, Aires V. Silymarin and cancer: A dual strategy in both in chemoprevention and chemosensitivity. Molecules. 2020; 25: 2009.
138. Moon YJ, Wang X, Morris ME. Dietary flavonoids: Effects on xenobiotic and carcinogen metabolism. Toxicol In Vitro. 2006; 20: 187-210.
139. Kiruthiga PV, Karthikeyan K, Archunan G, Pandian SK, Devi KP. Silymarin prevents benzo(a)pyrene-induced toxicity in wistar rats by modulating xenobiotic-metabolizing enzymes. Toxicol Ind Health. 2015; 31: 523-41.
140. Kawaguchi-Suzuki M, Frye RF, Zhu HJ, Brinda BJ, Chavin KD, Bernstein HJ, et al. The effects of milk thistle (silybum marianum) on human cytochrome p450 activity. Drug Metab Dispos. 2014; 42: 1611-6.
141. Upadhyay G, Kumar A, Singh MP. Effect of silymarin on pyrogallol- and rifampicin-induced hepatotoxicity in mouse. Eur J Pharmacol. 2007; 565: 190-201.
142. Zuber R, Modriansky M, Dvorak Z, Rohovsky P, Ulrichova J, Simanek V, et al. Effect of silybin and its congeners on human liver microsomal cytochrome p450 activities. Phytother Res. 2002; 16: 632-8.
143. Baer-Dubowska W, Szaefer H, Krajka-Kuzniak V. Inhibition of murine hepatic cytochrome p450 activities by natural and synthetic phenolic compounds. Xenobiotica. 1998; 28: 735-43.
144. Sridar C, Goosen TC, Kent UM, Williams JA, Hollenberg PF. Silybin inactivates cytochromes p450 3a4 and 2c9 and inhibits major hepatic glucuronosyltransferases. Drug Metab Dispos. 2004; 32: 587-94.
145. Beckmann-Knopp S, Rietbrock S, Weyhenmeyer R, Bocker RH, Beckurts KT, Lang W, et al. Inhibitory effects of silibinin on cytochrome p-450 enzymes in human liver microsomes. Pharmacol Toxicol. 2000; 86: 250-6.

146. Ahn K, Szczesna-Skorupa E, Kemper B. The amino-terminal 29 amino acids of cytochrome p450 2c1 are sufficient for retention in the endoplasmic reticulum. J Biol Chem. 1993; 268: 18726-33.
147. Galal AM, Walker LA, Khan IA. Induction of gst and related events by dietary phytochemicals: Sources, chemistry, and possible contribution to chemoprevention. Curr Top Med Chem. 2015; 14: 2802-21.
148. Maiorino M, Conrad M, Ursini F. Gpx4, lipid peroxidation, and cell death: Discoveries, rediscoveries, and open issues. Antioxid Redox Signal. 2018; 29: 61-74.
149. Bomgning CLK, Sinda PVK, Ponou BK, Fotio AL, Tsague MK, Tsafack BT, et al. Hepatoprotective effects of extracts, fractions and compounds from the stem bark of pentaclethra macrophylla benth: Evidence from in vitro and in vivo studies. Biomed Pharmacother. 2021; 136: 111242.
150. Grasselli E, Baldini F, Vecchione G, Oliveira PJ, Sardao VA, Voci A, et al. Excess fructose and fatty acids trigger a model of nonalcoholic fatty liver disease progression in vitro: Protective effect of the flavonoid silybin. Int J Mol Med. 2019; 44: 705-12.
151. Raza H. Dual localization of glutathione s-transferase in the cytosol and mitochondria: Implications in oxidative stress, toxicity and disease. FEBS J. 2011; 278: 4243-51.
152. Poruba M, Kazdova L, Oliyarnyk O, Malinska H, Matuskova Z, Tozzi Di Angelo I, et al. Improvement bioavailability of silymarin ameliorates severe dyslipidemia associated with metabolic syndrome. Xenobiotica. 2015; 45: 751-6.
153. Polachi N, Bai G, Li T, Chu Y, Wang X, Li S, et al. Modulatory effects of silibinin in various cell signaling pathways against liver disorders and cancer - a comprehensive review. Eur J Med Chem. 2016; 123: 577-95.
154. Quiroga AD, Lehner R. Pharmacological intervention of liver triacylglycerol lipolysis: The good, the bad and the ugly. Biochem Pharmacol. 2018; 155: 233-41.
155. Reid BN, Ables GP, Otlivanchik OA, Schoiswohl G, Zechner R, Blaner WS, et al. Hepatic overexpression of hormone-sensitive lipase and adipose triglyceride lipase promotes fatty acid oxidation, stimulates direct release of free fatty acids, and ameliorates steatosis. J Biol Chem. 2008; 283: 13087-99.
156. Kato M, Higuchi N, Enjoji M. Reduced hepatic expression of adipose tissue triglyceride lipase and cgi-58 may contribute to the development of non-alcoholic fatty liver disease in patients with insulin resistance. Scand J Gastroenterol. 2008; 43: 1018-9.
157. Wu JW, Wang SP, Alvarez F, Casavant S, Gauthier N, Abed L, et al. Deficiency of liver adipose triglyceride lipase in mice causes progressive hepatic steatosis. Hepatology. 2011; 54: 122-32.
158. Grabner GF, Xie H, Schweiger M, Zechner R. Lipolysis: Cellular mechanisms for lipid mobilization from fat stores. Nat Metab. 2021; 3: 1445-65.
159. Gluchowski NL, Gabriel KR, Chitraju C, Bronson RT, Mejhert N, Boland S, et al. Hepatocyte deletion of triglyceride-synthesis enzyme acyl coa: Diacylglycerol acyltransferase 2 reduces steatosis without increasing inflammation or fibrosis in mice. Hepatology. 2019; 70: 1972-85.
160. Amin NB, Carvajal-Gonzalez S, Purkal J, Zhu T, Crowley C, Perez S, et al. Targeting diacylglycerol acyltransferase 2 for the treatment of nonalcoholic steatohepatitis. Sci Transl Med. 2019; 11: eaav9701.
161. Rong S, Xia M, Vale G, Wang S, Kim CW, Li S, et al. DGAT2 inhibition blocks SREBP-1 cleavage and improves hepatic steatosis by increasing phosphatidylethanolamine in the ER. Cell Metab. 2024; 36: 617-29.e7.
162. Romeo S, Sanyal A, Valenti L. Leveraging human genetics to identify potential new treatments for fatty liver disease. Cell Metab. 2020; 31: 35-45.

163. Liu Z, Li H, Zheng Y, Gao Z, Cong L, Yang L, et al. Association of lipoprotein-associated phospholipase a2 with the prevalence of nonalcoholic fatty liver disease: A result from the apac study. Sci Rep. 2018; 8: 10127.
164. Sookoian S, Pirola CJ. Systematic review with meta-analysis: Risk factors for non-alcoholic fatty liver disease suggest a shared altered metabolic and cardiovascular profile between lean and obese patients. Aliment Pharmacol Ther. 2017; 46: 85-95.
165. Masoodi M, Gastaldelli A, Hyotylainen T, Arretxe E, Alonso C, Gaggini M, et al. Metabolomics and lipidomics in nafld: Biomarkers and non-invasive diagnostic tests. Nat Rev Gastroenterol Hepatol. 2021; 18: 835-56.
166. Haberl EM, Pohl R, Rein-Fischboeck L, Horing M, Krautbauer S, Liebisch G, et al. Hepatic lipid profile in mice fed a choline-deficient, low-methionine diet resembles human non-alcoholic fatty liver disease. Lipids Health Dis. 2020; 19: 250.
167. Sanyal AJ, Pacana T. A lipidomic readout of disease progression in a diet-induced mouse model of nonalcoholic fatty liver disease. Trans Am Clin Climatol Assoc. 2015; 126: 271-88.
168. Luukkonen PK, Qadri S, Ahlholm N, Porthan K, Mannisto V, Sammalkorpi H, et al. Distinct contributions of metabolic dysfunction and genetic risk factors in the pathogenesis of non-alcoholic fatty liver disease. J Hepatol. 2022; 76: 526-35.
169. Barbagallo I, Vanella L, Cambria MT, Tibullo D, Godos J, Guarnaccia L, et al. Silibinin regulates lipid metabolism and differentiation in functional human adipocytes. Front Pharmacol. 2015; 6: 309.
170. Zhu SY, Jiang N, Yang J, Tu J, Zhou Y, Xiao X, et al. Silybum marianum oil attenuates hepatic steatosis and oxidative stress in high fat diet-fed mice. Biomed Pharmacother. 2018; 100: 191-7.
171. Schriewer H, Kramer U, Rutkowski G, Borgis KJ. [influence of silybin-dihemisuccinate on fatty acid synthesis in rat liver (author's transl)]. Arzneimittelforschung. 1979; 29: 524-6.
172. Cui S, Pan XJ, Ge CL, Guo YT, Zhang PF, Yan TT, et al. Silybin alleviates hepatic lipid accumulation in methionine-choline deficient diet-induced nonalcoholic fatty liver disease in mice via peroxisome proliferator-activated receptor alpha. Chin J Nat Med. 2021; 19: 401-11.
173. Suguro R, Pang XC, Yuan ZW, Chen SY, Zhu YZ, Xie Y. Combinational applicaton of silybin and tangeretin attenuates the progression of non-alcoholic steatohepatitis (nash) in mice via modulating lipid metabolism. Pharmacol Res. 2020; 151: 104519.
174. Pferschy-Wenzig EM, Atanasov AG, Malainer C, Noha SM, Kunert O, Schuster D, et al. Identification of isosilybin a from milk thistle seeds as an agonist of peroxisome proliferator-activated receptor gamma. J Nat Prod. 2014; 77: 842-7.
175. Liu Y, Yu Q, Chen Y. Effect of silibinin on cflar-jnk pathway in oleic acid-treated hepg2 cells. Biomed Pharmacother. 2018; 108: 716-23.
176. Cui CX, Deng JN, Yan L, Liu YY, Fan JY, Mu HN, et al. Silibinin capsules improves high fat diet-induced nonalcoholic fatty liver disease in hamsters through modifying hepatic de novo lipogenesis and fatty acid oxidation. J Ethnopharmacol. 2017; 208: 24-35.
177. Ka SO, Kim KA, Kwon KB, Park JW, Park BH. Silibinin attenuates adipogenesis in 3t3-l1 preadipocytes through a potential upregulation of the insig pathway. Int J Mol Med. 2009; 23: 633-7.
178. Silva CM, Ferrari GD, Alberici LC, Malaspina O, Moraes KCM. Cellular and molecular effects of silymarin on the transdifferentiation processes of lx-2 cells and its connection with lipid metabolism. Mol Cell Biochem. 2020; 468: 129-42.

179. Salamone F, Galvano F, Cappello F, Mangiameli A, Barbagallo I, Li Volti G. Silibinin modulates lipid homeostasis and inhibits nuclear factor kappa b activation in experimental nonalcoholic steatohepatitis. Transl Res. 2012; 159: 477-86.
180. Vecchione G, Grasselli E, Voci A, Baldini F, Grattagliano I, Wang DQ, et al. Silybin counteracts lipid excess and oxidative stress in cultured steatotic hepatic cells. World J Gastroenterol. 2016; 22: 6016-26.
181. Xie Y, Feng SL, Mai CT, Zheng YF, Wang H, Liu ZQ, et al. Suppression of up-regulated lxralpha by silybin ameliorates experimental rheumatoid arthritis and abnormal lipid metabolism. Phytomedicine. 2021; 80: 153339.
182. Schriewer H. [increase in rat liver synthesis of fatty acids and glycerol phospholipids following parenteral application of silybin-dihemisuccinate]. Arzneimittelforschung. 1978; 28: 51-3.
183. Mourelle M, Franco MT. Erythrocyte defects precede the onset of ccl4-induced liver cirrhosis. Protection by silymarin. Life Sci. 1991; 48: 1083-90.
184. Schriewer H, Lohmann J. [disturbances in the regulation of phospholipid metabolism of the whole liver, mitochondria and microsomes in acute thioacetamide poisoning and the influence of silymarin]. Arzneimittelforschung. 1976; 26: 65-9.
185. Harayama T, Riezman H. Understanding the diversity of membrane lipid composition. Nat Rev Mol Cell Biol. 2018; 19: 281-96.
186. Valentine WJ, Yanagida K, Kawana H, Kono N, Noda NN, Aoki J, et al. Update and nomenclature proposal for mammalian lysophospholipid acyltransferases, which create membrane phospholipid diversity. J Biol Chem. 2021; 298: 101470.
187. Ramanathan R, Sivanesan K. Evaluation of ameliorative ability of silibinin against zidovudine and isoniazid-induced hepatotoxicity and hyperlipidaemia in rats: Role of silibinin in phase i and ii drug metabolism. Chem Biol Interact. 2017; 273: 142-53.
188. Villeneuve JP, Pichette V. Cytochrome p450 and liver diseases. Curr Drug Metab. 2004; 5: 273-82.
189. Leber HW, Knauff S. Influence of silymarin on drug metabolizing enzymes in rat and man. Arzneimittelforschung. 1976; 26: 1603-5.
190. Rajnarayana K, Reddy MS, Vidyasagar J, Krishna DR. Study on the influence of silymarin pretreatment on metabolism and disposition of metronidazole. Arzneimittelforschung. 2004; 54: 109-13.
191. Tighe SP, Akhtar D, Iqbal U, Ahmed A. Chronic liver disease and silymarin: A biochemical and clinical review. J Clin Transl Hepatol. 2020; 8: 454-8.
192. Xiao F, Gao F, Zhou S, Wang L. The therapeutic effects of silymarin for patients with glucose/lipid metabolic dysfunction: A meta-analysis. Medicine (Baltimore). 2020; 99: e22249.

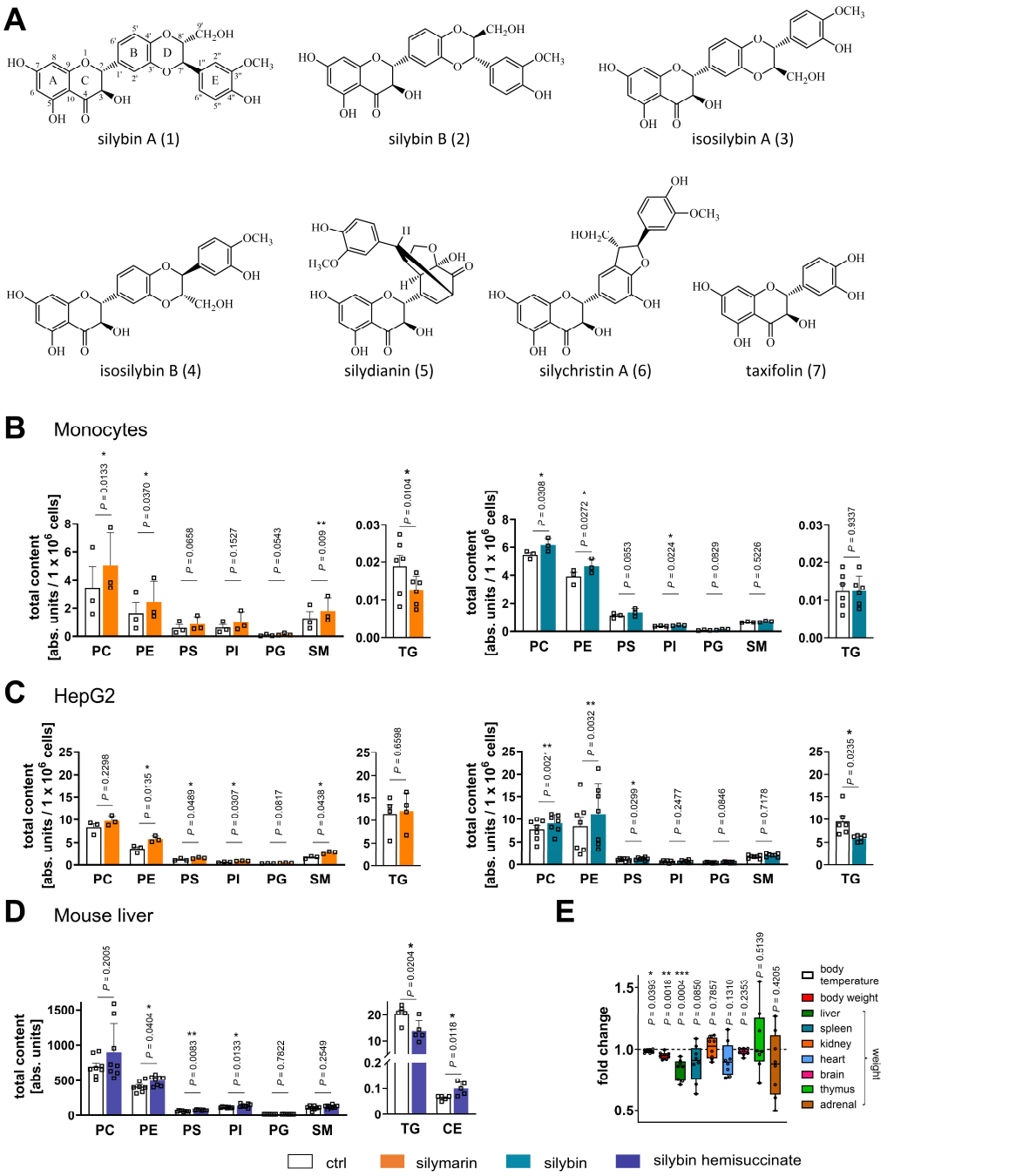

Figure 1. Shift from TGs to phospholipids in human monocytes, hepatocytes, and mouse liver. (A) Main components of silymarin. (B-D) Total amounts of lipid classes were determined by UPLC-MS/MS. (B, C) Human primary monocytes (B) and HepG2 cells (C) were treated with silymarin (50 µg/ml for monocytes and 10 µg/ml for HepG2 cells), silybin (20 µM), or vehicle (ethanol for silymarin, DMSO for silybin) for 24 h. Individual values and mean + SEM; n = 3 (B: except TG, C: silymarin except TG), n = 4 (C: TG silymarin), n = 6 (B: TG silymarin and silybin, C: TG silybin), n = 7 (C: silybin except TG). (D, E) Mice received silybin hemisuccinate ('silybin'; 200 mg/kg, i.p.) or vehicle (0.9% NaCl) trice at 0, 12, and 24 h and were sacrificed after 37 h. (E) Body temperature, body weight and organ weight of mice upon administration of silybin. Temperature and body weight were measured after 37 h before animals were sacrificed and organs collected. The box-and-whisker plot shows fold-changes upon silybin gavage. The median fold change belonging to each group is shown as bold line. The boxes extend from the 25th to 75th percentiles, and whiskers extend to minimal and maximal values. Vehicle control; body temperature: 37.2 ± 0.2 [°C]; body weight: 21.9 ± 0.2 [g]; liver: 1.31 ± 0.03 [g]; spleen: 0.070 ± 0.002 [g]; kidney: 0.1445 ± 0.004 [g]; heart: 0.126 ± 0.0023 [g]; brain: 0.439 ± 0.006 [g]; thymus: 0.049 ± 0.002 [g]; adrenal: 0.0105 ± 0.001 [g]; Lipid contents are given as nmol / 1×10^6 cells for PC and units / 1×10^6 cells for PE, PS, PI, PG, SM and TG. Individual values and mean + SEM (D) or box plots and individual values (E) from n = 5 (D: CE and TG), n = 7 (D: PE; ctrl, E: body temperature), n = 8 (D: except CE and TG, E: body and organ weights) mice/group. *P < 0.05, **P < 0.01, ***P < 0.001 vs. vehicle control. Two-tailed paired (B, C) or unpaired (D, E) Student's *t*-test.

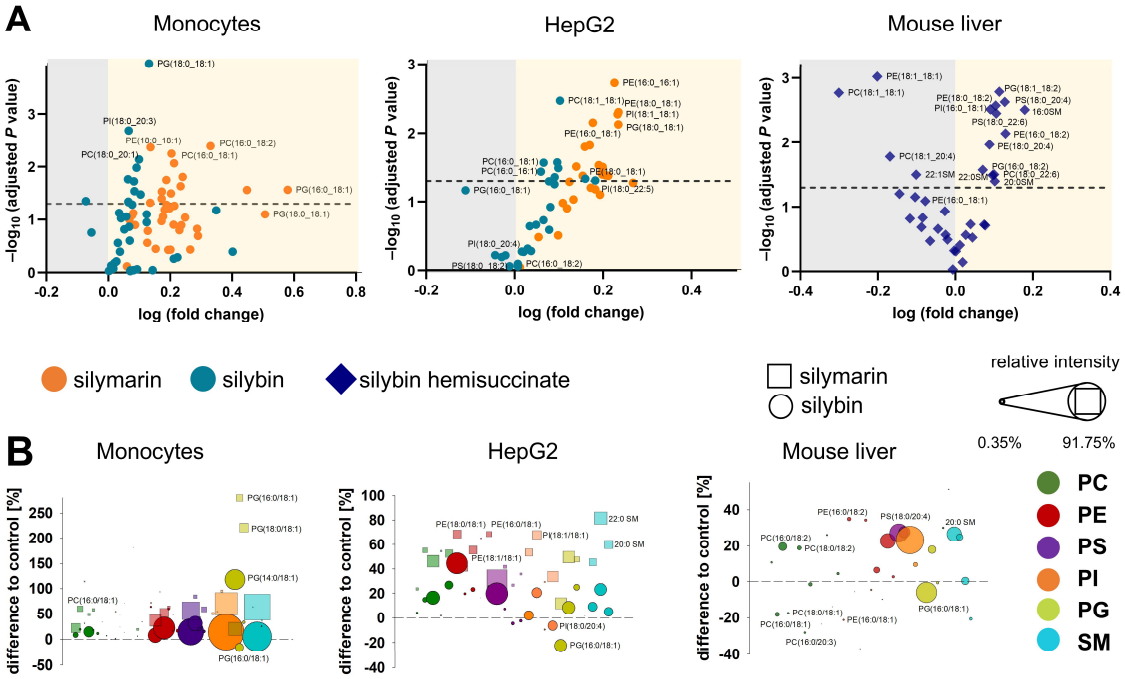

Figure 2. Phospholipid profiling indicates an upregulation of diverse species. Human primary monocytes and HepG2 cells were treated with silymarin (50 µg/ml for monocytes and 10 µg/ml for HepG2 cells), silybin (20 µM) or vehicle (ethanol for silymarin, DMSO for silybin) for 24 h. Mice received silybin hemisuccinate ('silybin'; 200 mg/kg) or vehicle (0.9% NaCl) trice at 0, 12, and 24 h and were sacrificed after 37 h. (A) Volcano plots showing the cellular proportion of phospholipid species that increase (yellow background) or decrease (grey background) upon treatment with silymarin or silybin. Adjusted *P* values given vs. vehicle control. The dashed line indicates a *P*-value of 0.05. (B) Forest plots depicting phospholipid species that are up- (positive values) or down-regulated (negative values) by silymarin (squares) or silybin (circles). Values, calculated as percentage of control, show the difference to 100%, with the dashed line at 0% indicating no difference to control. The dot size describes the mean relative abundance of phospholipid species within the phospholipid subclass (relative intensities). Data and the number of experiments are identical to Figure 1.

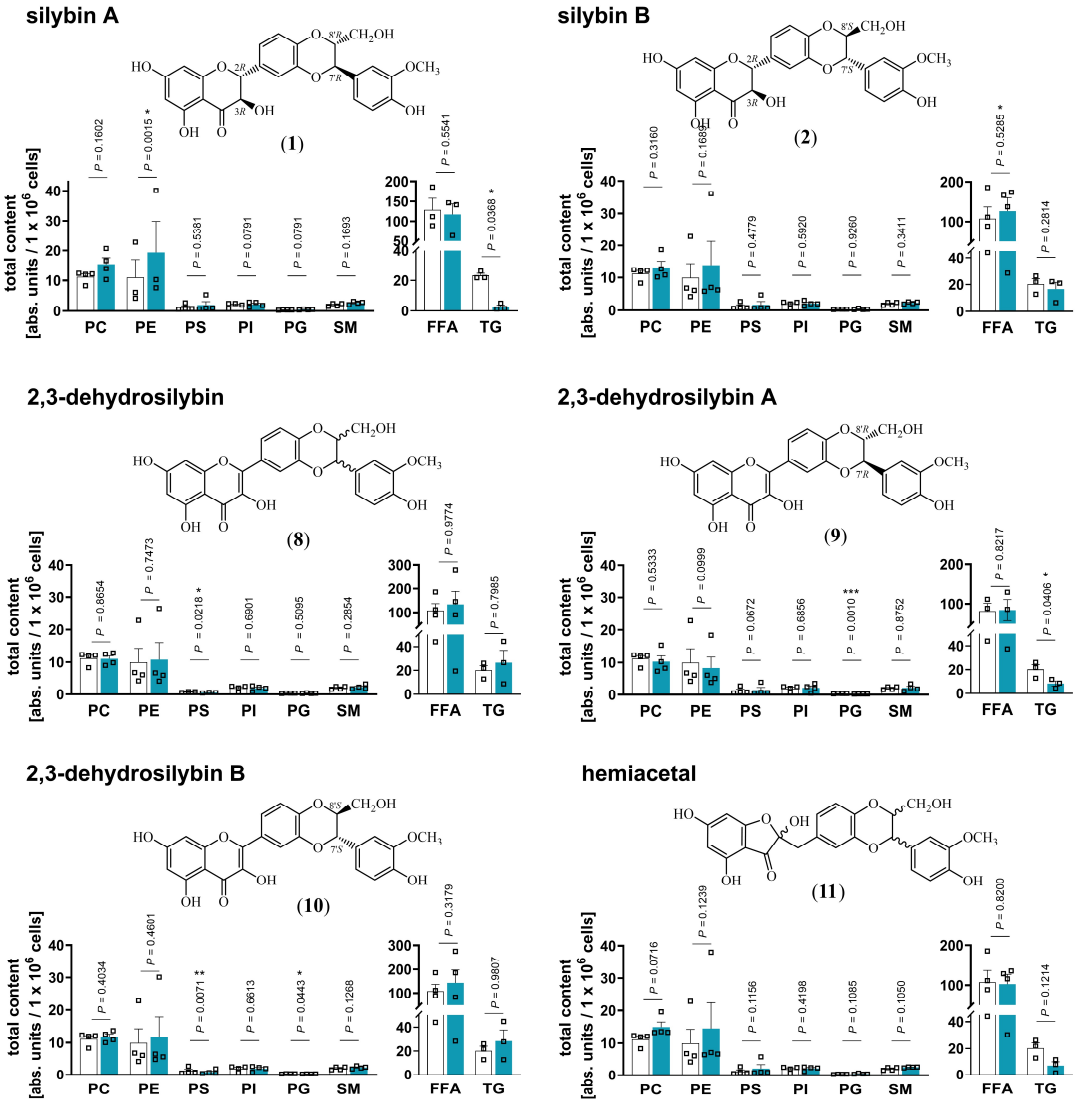

Figure 3. Silybin A is the active isomer that causes the switch from TGs to phospholipids. HepG2 cells were treated with the indicated compounds (20 µM) or vehicle (DMSO) for 24 h. Total amounts of lipid classes were determined by UPLC-MS/MS and are given as nmol / 1×10^6 cells for PC and units / 1×10^6 cells for PE, PS, PI, PG, SM and TG. Individual values and mean + SEM; n = 3 (PE silybin A, PS dehydrosilybin, TGs, free fatty acids (FFA) 2,3-dehydrosilybin A and B) n = 4 (except PE silybin A, PS dehydrosilybin, TGs, free fatty acids FFA 2,3-dehydrosilybin A and B). $^*P < 0.05$, $^{**}P < 0.01$, $^{***}P < 0.001$ vs. vehicle control (DMSO). Two-tailed paired Student's *t*-test of log-transformed data.

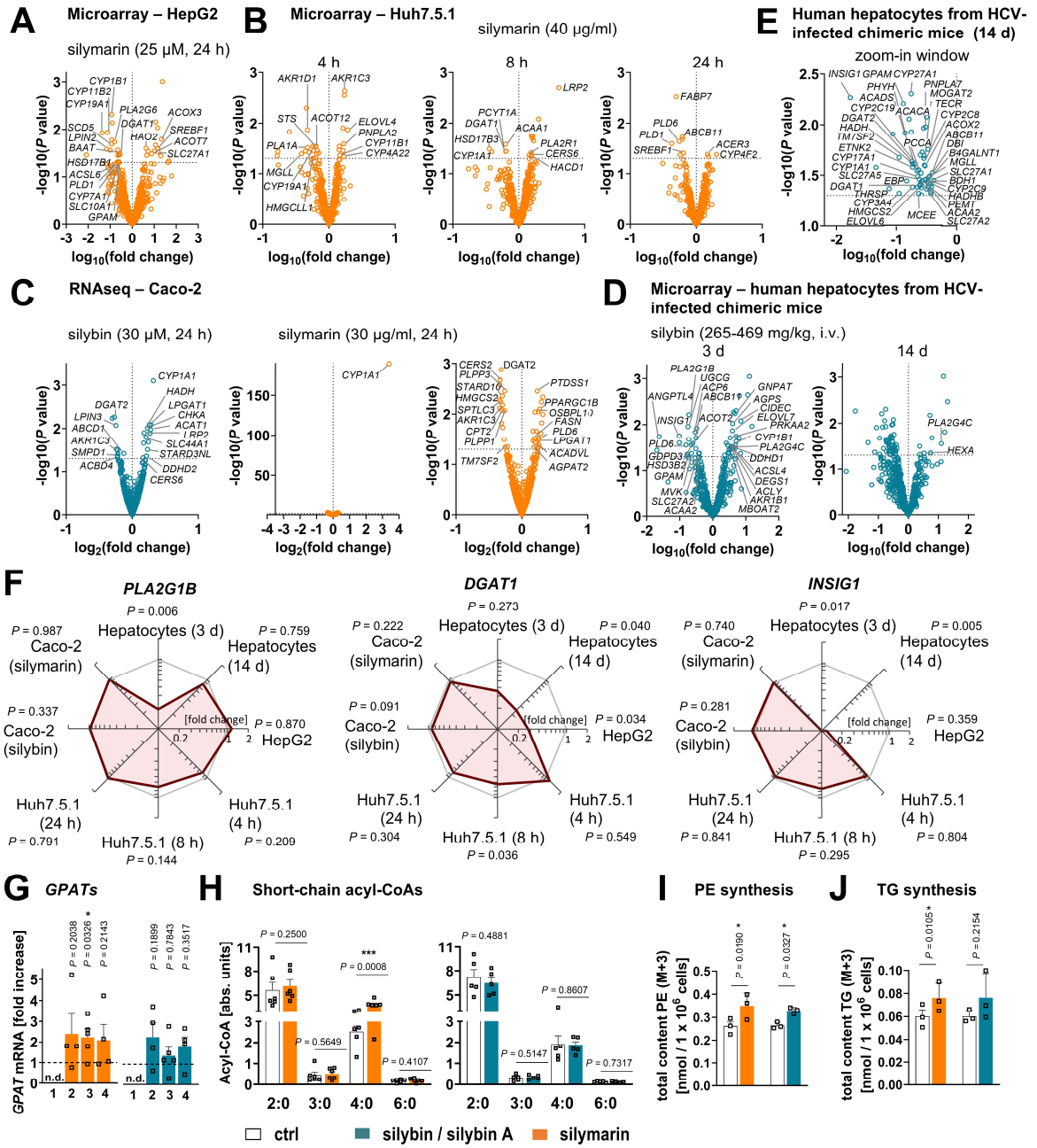

Figure 4. Silymarin/silybin induces global changes in phospholipid, TG and sterol metabolism. (A-F) Comparative analysis of transcriptome data from silymarin-treated HepG2 (A) and Huh7.5.1 hepatocarcinoma cells (B), silymarin- and silybin-treated Caco-2 colon carcinoma cells (C), and hepatocytes derived from HCV-infected mice receiving silybin (D, E). Volcano plots compare the expression of lipid metabolic genes upon silymarin (A-C) or silybin (C-E) treatment vs. vehicle control. Differentially expressed genes are defined as those that show consistent regulation in the same direction in at least two independent model systems at a significance level of $P < 0.05$ (without adjustment for multiple comparisons) and are annotated in the corresponding plots. The dashed line indicates a *P*-value of 0.05; multiple two-tailed unpaired Student's *t*-tests. (F) Radar plots indicating the fold change in *PLA2G1*, *DGAT1*, and *INSIG1* expression by silymarin (HepG2, Huh7.5.1, Caco-2) or silybin (hepatocytes, Caco-2) relative to vehicle control. Non-adjusted *P* values given vs. vehicle control; multiple two-tailed unpaired Student's *t*-tests (G-J). HepG2 cells were incubated with silymarin (10 µg/ml), silybin (20 µM) or vehicle (ethanol for silymarin, DMSO for silybin) for 24 h. (G) mRNA levels of *GPAT2-4* normalized to β-actin. Individual values and mean + SEM as fold-change of control; n = 4 (GPAT2 and GPAT4), n = 5 (*GPAT3*). (H) Effects of silymarin and silybin on the cellular ratio of short-chain acyl-CoAs, normalized to the internal standard [$^{13}C_3$]-malonyl-CoA. Individual values and mean + SEM; n = 5 (silybin) and n = 6 (silymarin). *$P < 0.05$, ***$P < 0.001$ vs. vehicle controls; two-tailed paired Student's *t*-tests. (I, J) Incorporation of isotopically labeled sodium acetate-$^{13}C_2$, d_3 in PE (I) and TG (J) by HepG2 cells treated with silymarin (10 µg/ml), silybin (20 µM), or vehicle (ethanol for silymarin, DMSO for silybin) for 24 h. The total amount of the isotopically labeled PE and TG species analyzed is shown. Individual values and means + SEM; n = 3. *$P < 0.05$ vs. vehicle controls; two-tailed paired Student's *t*-tests.

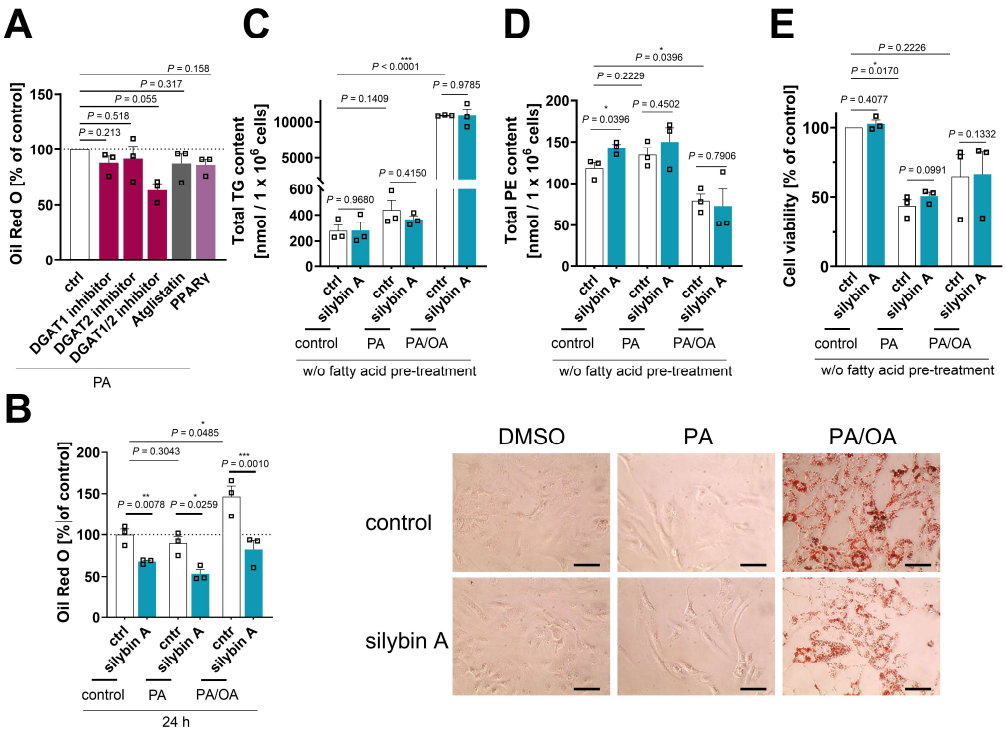

Figure 5. The efficacy of silybin in inducing a lipid class switch differs between hepatocyte pre-disease and disease models. (A,B) HepaRG cells were treated with 0.1 mM palmitate (PA) or a mixture of PA/oleate (OA) in a 1:2 ratio (in total 1 mM) together with vehicle (DMSO, 0.5%), silybin A (20 µM), the ATGL inhibitor atglistatin (50 µM), the DGAT1 inhibitor A 922500 (5 µM), the DGAT2 inhibitor PF-06424439 (10 µM), a combination of DGAT1 (5 µM) and DGAT2 inhibitors (10 µM), or the PPARγ antagonist GW9662 (5 µM) for 24 h. (A) Relative lipid droplet content. Individual values and mean + SEM, n = 3. (B) Left panel: Relative lipid droplet content. Individual values and mean + SEM, n = 3. Right panel: Representative images of HepaRG cells stained for lipid droplets using Oil Red O; scale bar, 50 µm. (C, D) HepaRG cells were co-treated directly with with 0.1 mM palmitate (PA) or a mixture of PA/oleate (OA) in a 1:2 ratio (in total 1 mM) and vehicle (DMSO, 0.5%) or silybin A (20 µM) for 24 h. Total levels of TG (C) and PE (D) determined by UPLC-MS/MS. Individual values and mean + SEM, n = 3. (E) Cell viability measured by MTT assay. Individual values and mean + SEM, n = 3. *$P < 0.05$, **$P < 0.01$, ***$P < 0.001$ vs. control; two-tailed paired (A, B, E) or unpaired (C, D) Student's *t*-test.

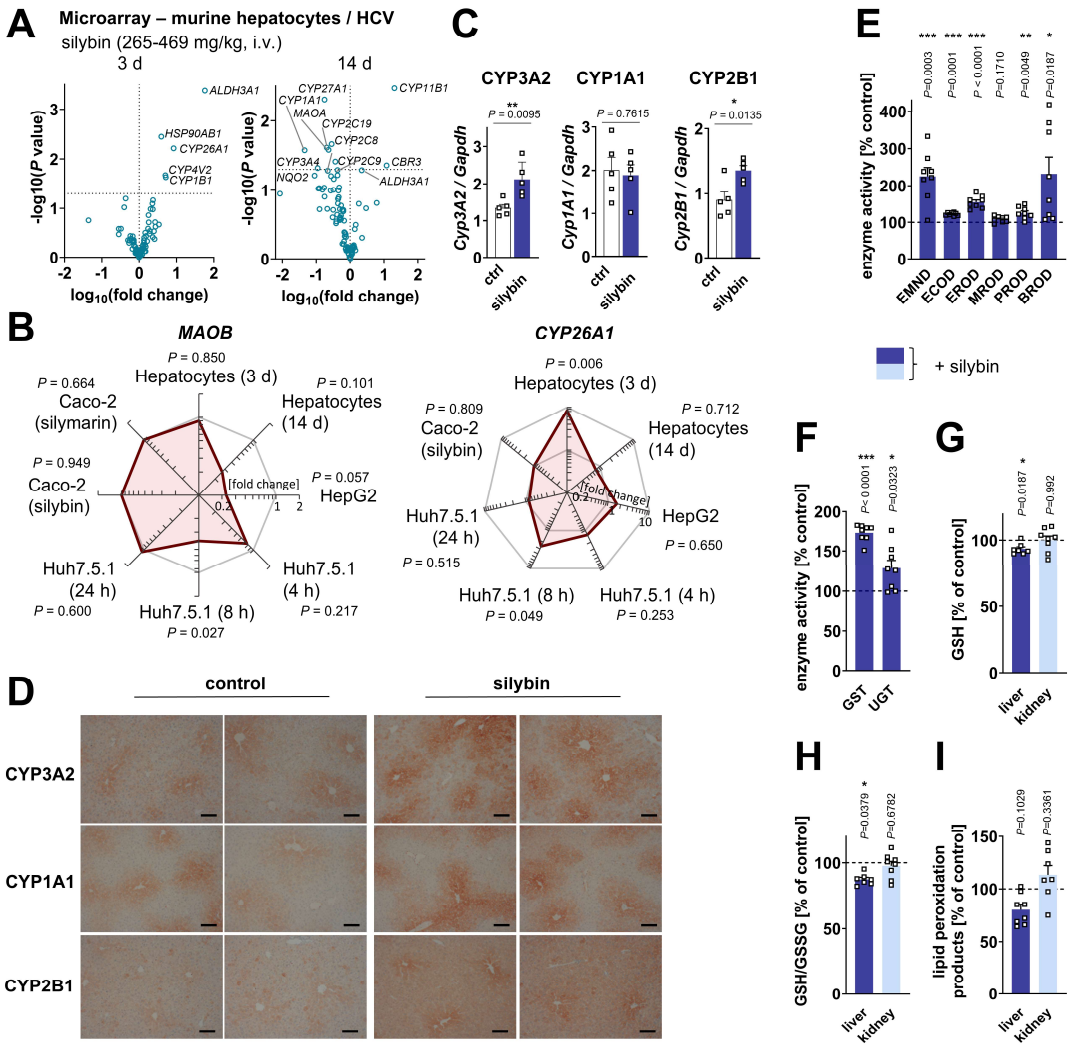

Figure 6. Elevated *CYP* enzyme expression and activity in mouse liver. (A) Comparative analysis of transcriptome data from hepatocytes derived from silybin-treated HCV-infected mice. Volcano plots compare the expression of lipid metabolic genes upon silybin treatment vs. vehicle control at day 3 and day 14. The dashed line indicates a non-adjusted *P*-value of 0.05; multiple two-tailed unpaired Student's *t*-tests. (B) Radar plots indicating the fold change in *MAOB* and *CYP26A1* expression by silybin relative to vehicle control. Non-adjusted *P* values given vs. vehicle control; multiple two-tailed unpaired Student's *t*-tests. (C-I) Mice received silybin hemisuccinate ('silybin'; 200 mg/kg, i.p.) or vehicle (0.9% NaCl) trice at 0, 12, and 24 h and were sacrificed after 37 h. (C) Protein expression of CYP3A2, CYP1A1, and CYP2B1 in mouse liver homogenates. Representative Western blots are shown in Figure S16. Individual values and mean + SEM; n = 5 mice/group. (D) Immunohistological analysis of CYP3A2, CYP1A1 and CYP2B1 expression in mouse liver; scale bar, 100 µm. n = 5 mice/group. (E) CYP activity measured by detecting the oxidative demethylation product formaldehyde (EMND) or the conversion of fluorogenic substrates in mouse liver homogenates. EMND: *N*-ethylmorphine *N*-demethylation (CYP3A), ECOD: 7-ethoxycoumarin *O*-deethylation (CYP1A and CYP2A-C), EROD: 7-ethoxyresorufin *O*-deethylation (CYP1A), MROD: 7-methoxyresorufin *O*-demethylation (CYP1A), PROD: 7-pentoxyresorufin *O*-dependentylation (CYP2B), BROD: 7-benzyloxyresorufin *O*-debenzylation (CYP2A-C and CYP3A). Indicative CYP enzymes are listed in brackets. Individual values and mean + SEM; n = 8 mice/group. (F) Enzyme activity of GST and UGT in mouse liver homogenates. GST: gluthathione *S*-transferase; UGT: UDP-glucuronosyltransferase. Individual values and mean + SEM; n = 8 mice/group. (G-I) GSH levels (G), GSH/GSSG ratio (H) and lipid peroxidation (I) in mouse liver and kidney homogenates. Individual values and mean + SEM; n = 7 (liver GSH and GSH/GSSG, kidney lipid peroxidation) or n = 8 (kidney GSH and GSH/GSSG, liver lipid peroxidation) mice/group. **P* < 0.05, ***P* < 0.01, ****P* < 0.001 vs. control; two-tailed unpaired Student's *t*-test.

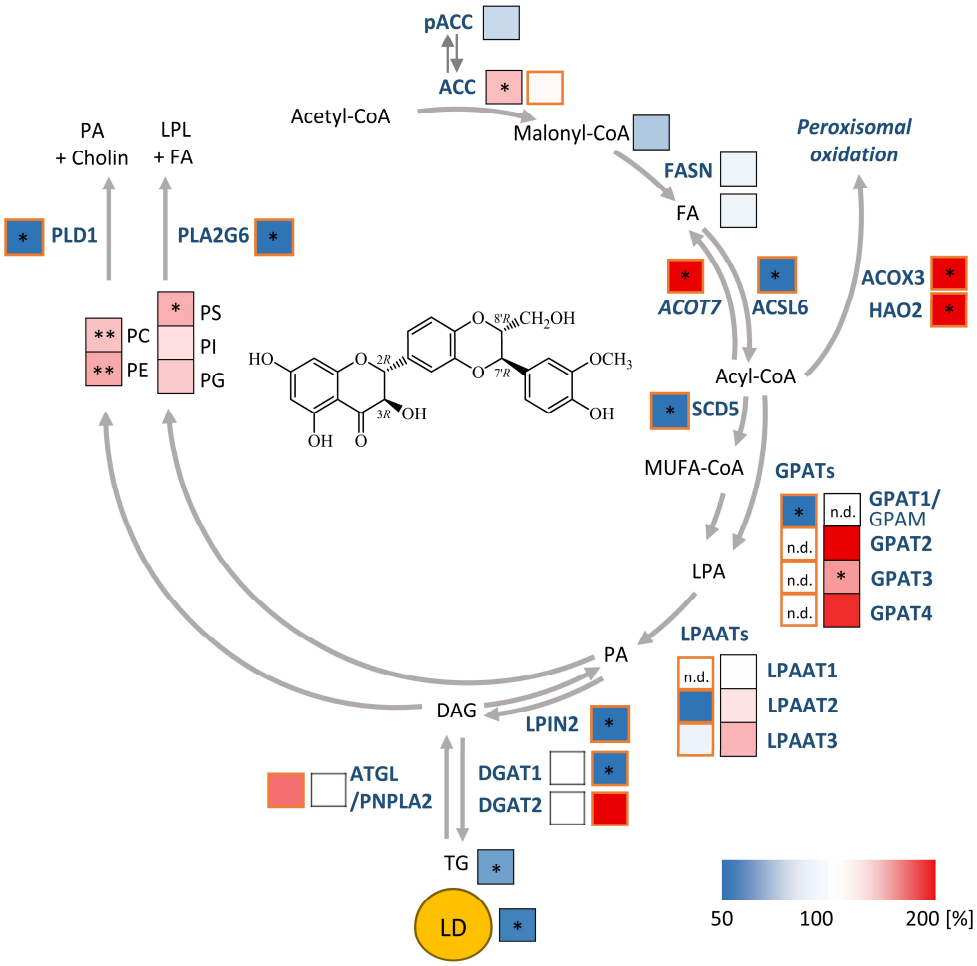

Figure 7. Proposed mechanisms of silymarin and its bioactive constituent silybin A in hepatocytes. Acetyl-CoA-carboxylase (ACC/ACACA) converts acetyl-CoA to malonyl-CoA, which is elongated to long-chain fatty acids by fatty acid synthase (FASN). Acyl-CoA esters are formed from free fatty acids (FAs) by acyl-CoA synthetases (ACSLs), which also activate exogenous fatty acids for further metabolism. Saturated acyl-CoAs are converted into monounsaturated acyl-CoAs (MUFA-CoA) preferentially by Δ9-desaturases, such as the stearoyl-CoA desaturase (SCD) isoenzyme 5. Acyl-CoA thioesterases (ACOTs) catalyze the opposite reaction, hydrolyzing acyl-CoAs to free fatty acids (FAs). Acyl-CoAs are used by glycerol-3-phosphate acyltransferases (GPATs) and lysophospholipid (LPL) acyltransferases/lysophosphatidic acid acyltransferases (LPLATs/LPAATs) to introduce fatty acyl-chains into the *sn*-1 and *sn*-2 positions of glycerol-3-phosphate and lysophosphatidic acid (LPA), respectively. The resulting PA is either converted to CDP-DAG for PI, PG, and PS biosynthesis or dephosphorylated to DAG for TG, PC, and PE biosynthesis by lipins (LPINs) and other PA phosphatases. LPIN2 also plays an important role in the regulation of fatty acid metabolism as nuclear transcriptional coactivator. Acylation of DAG by DGATs yields TGs, which are stored in lipid droplets and mobilized by ATGL/PNPLA2 and other triglyceride lipases, providing DAG and FAs. Phospholipid degradation is driven by a large number of phospholipases with different specificities. PLA2G6 releases saturated and unsaturated long-chain fatty acids from the *sn*-1 or *sn*-2 position of phospholipids, such as PC, PE and PA, whereas PLD1 specifically cleaves PC to PA and choline. By targeting multiple nodes, silymarin/silybin triggers a switch from TGs to phospholipids, thereby enriching intracellular membranes with phospholipids that have a balanced fatty acid composition. The increase in intracellular membranes is associated with enhanced membrane-associated biotransformation capacities. Mechanistically, silymarin/silybin inhibits phospholipid degradation, while moderately activating *de novo* phospholipid biosynthesis and stimulating TG catabolism in lipid droplets (LD), which in combination results in an effective channeling of TG-derived DAG and FAs into membrane biogenesis. In addition, silymarin induces the expression of genes involved in peroxisomal fatty acid degradation (HAO2, ACOX3), upregulates ACOT7, which hydrolyzes acyl-CoAs into FAs and CoA, and decreases the expression of ACSLs, that activate long-chain fatty acids. The color scale in the pathway diagram indicates the percentage changes in metabolite levels, lipid droplet counts, and enzyme expression by silybin relative to vehicle control in HepG2 cells (black bordered boxes) or by silymarin relative to vehicle control in HepG2 cells (orange bordered boxes). GPAM, glycerol-3-phosphate acyltransferase, mitochondrial.